EXPERIMENTAL MEASUREMENT OF PHASE AVERAGED WALL-PRESSURE DISTRIBUTIONS FOR A 25% ECCENTRIC WHIRLING ANNULAR SEAL

A Thesis

by

DOMENIC CUSANO

Submitted to the Office of Graduate Studies of
Texas A&M University
in partial fulfillment of the requirements for the degree of

MASTER OF SCIENCE

May 2006

Major Subject: Mechanical Engineering

EXPERIMENTAL MEASUREMENT OF PHASE AVERAGED WALL-

PRESSURE DISTRIBUTIONS FOR A 25% ECCENTRIC WHIRLING

ANNULAR SEAL

A Thesis

by

DOMENIC CUSANO

Submitted to the Office of Graduate Studies of
Texas A&M University
in partial fulfillment of the requirements for the degree of

MASTER OF SCIENCE

Approved by:

Chair of Committee,	Gerald L. Morrison
Committee Members:	Dara W. Childs
	Robert E. Randall
Head of Department:	Dennis L. O'Neal

May 2006

Major Subject: Mechanical Engineering

ABSTRACT

Experimental Measurement of Phase Averaged Wall-Pressure Distributions for a 25%
Eccentric Whirling Annular Seal. (May 2006)
Domenic Cusano, B.S., Texas A&M University
Chair of Advisory Committee: Dr. Gerald L. Morrison

Instantaneous wall-pressure data were recorded for a 25% eccentric whirling annular seal
for rotor speeds of 1800RPM and 3600RPM, axial Reynolds numbers of 24000 and
12000, and whirl ratios of 0.1-1.0 following the procedure set forth by Winslow (1994),
Robic (1999) and Suryanarayanan (2003). Overall, the phase averaged wall-pressure
distributions were consistent with previous results. The "switch" in the pressure
distribution measured by Suryanarayanan (2003) and Robic (1999) from pressure to
suction between the seal entrance and exit occurs at and above a whirl ratio of 0.7 for
1800RPM and 0.4 for 3600RPM. For both rotor speeds, decreasing the flow rate by one-
half also decreases the wall pressure fluctuation distributions by one-half. For whirl
ratios less than 0.5, the phase averaged pressure field was relatively constant which leads
to minimal forces being imparted on the rotor by the fluid in the annulus. Talyor-Gortler
vortices are measured for 1800RPM and Re=24000 at whirl ratios 0.1 and 0.3-0.7. As
the whirl ratio increases past 0.5, longitudinal vortices begin to emerge in the pressure
contours and skew axially with 180° shifts occurring when the Taylor-Reynolds ratio is
large enough. Longitudinal vortices were measured for both rotor speeds when the
whirling motion is greater than 1400RPM for Re=12000 and greater than 1600RPM for
Re=24000. Attempts were made to apply Childs (1983) procedure for finding the
rotordynamic coefficients of annular seals; however, the seal moves in a non-circular
orbit about the seal's center so Childs analysis cannot be applied.

DEDICATION

This work is dedicated to my parents and family; thanks for never giving up on me.

ACKNOWLEDGMENTS

TABLE OF CONTENTS

LIST OF FIGURES

NOMENCLATURE

c - Clearance (1.27mm)

$\widetilde{C}, \widetilde{c}$ - Dimensionless direct and cross-coupled damping coefficients

$C_P = \dfrac{P^* c^2}{6\mu\omega R}$ - Sommerfeld journal bearing pressure coefficient

C_i - Percent of one complete whirl cycle

E - Young's modulus

F_x - Reaction-force (x-direction) acting on rotor

F_y - Reaction-force (y-direction) acting on rotor

$\widetilde{K}, \widetilde{k}$ - Dimensionless direct and cross-coupled stiffness coefficients

L - Seal length (35.56mm)

$n_o = 0.079$ - Coefficient from Hirs' (1973) turbulence equations

$m_o = -0.25$ - Coefficient from Hirs' (1973) turbulence equations

$\widetilde{M}, \widetilde{m}$ - Dimensionless direct and cross-coupled mass coefficients

P^* - AC pressure

P^*_{mean} - DC mean pressure

P - Phase averaged pressure

P_{in}, P_{out} - Inlet and outlet phase averaged pressures

$\overline{P}$ - Mean pressure

ΔP - Seal differential pressure

Q - Flow rate through seal (L/s)

R - Seal radius (164mm)

$R_o = \varepsilon c$ - Amplitude of seal harmonic motion

$\mathrm{Re} = \dfrac{2\rho V c}{\mu}$ - Axial Reynolds number

$T = L / V$ - Transit time of fluid element proceeding through seal

t - Time

$$Ta = \frac{\rho W_{sh} c / \mu}{\sqrt{2c/D}}$$ - Taylor number

V - Mean axial velocity (m/s)

W_{sh} - Rotor surface velocity (m/s)

Z - Downstream distance from seal inlet

α - Coefficient of thermal expansion

β - Whirl ratio

ε - Dimensionless eccentricity ratio

ρ - Density of water (kg/m^3)

λ - Friction-loss coefficient from Childs (1983)

σ_{ult} - Ultimate strength

ω - Rotor angular speed (rad/s)

Ω - Whirl angular speed (rad/sec)

$\mu = 7.84*10^{-4} \, kg/m \cdot s$ - Absolute viscosity

ν - Kinematic viscosity

INTRODUCTION

The purpose of seals in Turbomachinery design is to prevent, or minimize, leakage from a region of high pressure to a region of lower pressure. The two basic types of seals which are studied extensively are smooth and labyrinth annular seals. Labyrinth seals are characterized by a series of thick grooves cut into the circumference of the seal whereas smooth annular seals are characterized by a smooth surface around the circumference. While surface treatments for annular seals are available, the smooth annular seal is studied in this analysis.

Instabilities of rotors can occur due to mechanical wear, improper balancing of components, or failing to comply with design speeds. A phenomenon specific to design speeds is whirl instability. Whirl instability occurs when the rotor deviates from journal bearing operation and begins to oscillate within the stator housing in a periodic orbit. Newkirk and Taylor (1925) were the first to study the phenomenon, and found that the rotor begins uncontrolled oscillations within the stator when the rotor speed reaches twice the critical speed. The critical speed occurs when the rotor operating speed matches that of the damped natural frequency and is characterized by heavy rotor vibrations.

The hydrodynamic forces within a whirling ('whipping') annular seal are unique. Previous investigations by Winslow (1994), Robic (1999), and Suryanarayanan (2003) experimentally measured the wall pressure distribution along an annular seal. The most significant finding is that the pressure distribution switches position from the upstream seal inlet to the downstream seal exit under certain operating conditions. Measurements of the phase averaged pressure distribution along the length of the seal give an idea as to what forces are inherent on the rotor at different whirl ratios (whirling speeds).

The purpose of this project is to investigate the effect of whirl ratio on the pressure distribution within an annular seal and to find the effect, if any, on the rotordynamic

_____

This thesis follows the style and format of *Journal of Turbomachinery*.

coefficients due to whirl ratio for two shaft speeds and flow rates. The objectives of this investigation are to:

1. Measure the stator wall pressure inside a dynamically eccentric whirling annular seal

2. Obtain phase averaged wall-pressure distributions inside the seal for whirl ratios 0.1-1.0 in 0.1 increments for 1800rpm and 3600rpm at Re=12,000 and 24,000.

3. Plot phase averaged pressure distributions and create carpet plots for percent cycle and downstream position.

4. Integrate pressure distributions to determine the force exerted on rotor as a function of whirl ratio

5. Obtain rotordynamic coefficients as a function of operating conditions.

If there is an effect of operating conditions on the rotordynamic coefficients of turbulent annular seals, the author hopes that this paper will serve to assist in re-linking experiments and numerical solutions for whirling annular seals.

LITERATURE REVIEW

Newkirk and Taylor (1925) referred to the action of whirl instabilities as "oil whip," due to the apparent dependence of oil film forces in contributing to the whipping of the shaft at rotor speeds over twice the critical speed. Using multiple arrangements and bearing weights to change critical rotor speeds, Newkirk and Taylor measured the motion of a rotor tip and found that violent whipping, or whirling, occurred at speeds around twice the critical. It was also discovered that the whirling motion occurred in the same direction as the rotor motion. Newkirk and Taylor accidentally discovered that oil film forces were a large contributor to oil whip since the whipping would stop immediately when the oil supply to the bearing was shut off and could be brought back to full amplitude by turning on the oil supply again. The overall recommendations by Newkirk and Taylor to prevent oil whip is to (1) shut off oil to the bearing, (2) steadying the shaft with additional weight, (3) misalign the bearings, (4) keeping operating speeds below twice the critical, (5) use of friction-damped bearings, and (6) avoiding very light bearing loading pressures.

Future investigations into the onset of whirl instabilities began as a problem of understanding first, the forces imparted on the rotor to grasp ranges of stable and unstable operation, then second, the effect of fluid flow interactions with the rotor. Therefore, most of the first published accounts after Newkirk and Taylor focus on understanding both fluid flows inside the seal as well as the effect of the flow field on the rotordynamic characteristics of the rotor system. It is for this reason that the remaining publications are divided into primarily fluid flow investigations and rotordynamic characteristic investigations; even though the problem of whirl instabilities is a combination of the two.

Fluid Flow Investigations

DiPrima and Stuart (1972) derived the Sommerfeld Journal Bearing Pressure Distribution equation from the Navier-Stokes equations and attempted to calculate curvature and

inertial corrections for flow in a journal bearing. It was found that viscous terms do not contribute to the normal stress but does contribute to shear stress. As a consequence of the inertial correction factor, the shaft center will not be oriented in a horizontal line as predicted by the Sommerfeld Pressure Distribution. DiPrima and Stuart attribute this to an additional force perpendicular to the Sommerfeld field force due to the inertial correction factor. Finally, the curvature correction gives a small correction to the Sommerfeld pressure distribution but the significance of the curvature is dependent on the eccentricity of the annulus.

Hirs (1973) developed a bulk-flow model for turbulent flow in lubricant films interposed between smooth surfaces. To model fluid flow between concentric cylinders, no knowledge of the flow velocity profiles are needed to derive the empirical constants; only bulk-flow measurements. When compared to mixing length and law-of-wall theories, Hirs found that his bulk-flow model agrees with law-of-wall theory for turbulent flow in bearing films at greater Reynolds numbers with marginal to improved utilization in lower Reynolds number conditions (Hirs does not give magnitudes for what is considered greater/lower Reynolds numbers).

Brennen (1976) investigated the lack of information on the nature of flow and forces in an annulus between coaxially cylinders where either or both are performing whirling motions. Brennens' paper was the first to analytically determine the dependence of whirl motion on flow conditions. Interactions between the fluid lubricant and the rotor is a function of the whirl deflection of the intermediate casing, which Brennen notes, is in turn a function of the forces imparted by the fluid motions in the outer annulus. Brennen suggests the possibility of whirl instabilities at sub-synchronous frequencies and that for high flow Reynolds flow the mean flow will become unstable to Taylor vortices above a critical Taylor number.

Recent research into the flow fields inside eccentric and whirling annular seals began when Johnson (1989) and Morrison et. al (1994) developed a pioneering laser measurement system at the Turbomachinery Laboratory at Texas A&M University.

Johnson performed detailed flow measurements for both smooth and labyrinth annular seals. It was found that there is a small entrance region where the radial velocity decays from 0.08U to zero in the first x/c=1 of the seal. This effect, later confirmed by Thames (1992) and reported by Morrison et. al, was concluded to be a contribution of *vena contracta*. Thames also confirmed the recirculation zone ('saddle back' effect) discovered by Johnson, with measurements of the peak axial velocity; the peak axial velocity that was located on the suction side of the clearance at the seal inlet rotated around to the pressure side of the clearance at the seal exit.

Das (1993) was the first researcher to investigate modified eccentricities with the Turbomachinery Laboratory test-rig. Where previous research by Johnson and Thames investigated synchronous whirl at 50% eccentricity, Das operated at a 10% eccentricity. The saddle-back effect was not as large in the 10% eccentricity case as it had been in the 50% eccentric case and was attributed to the seal clearance of the rotor. Das concluded that the diminished effect of the rotor eccentricity develop earlier for small eccentricities due to a lower amount of pre-swirl.

Winslow (1994) and Morrison and Winslow (1995) experimentally measured the dynamic pressure and shear stress on the stator wall for 0, 10, and 50% eccentric annular seals and found that in the case of lower eccentricities, such as in Das' analysis, there are small entrance and exit affects whereas in the case of higher eccentricities, such as in Thames' analysis, there is a marked peak in the mean pressure followed by a gradual decay until near the seal exit where the pressures begin to increase again. Contour and carpet plots of the phase averaged fluctuations show that the highest entrance pressure reside on the pressure side of the seal and the lowest pressures reside on the suction side; but that at the exit these pressure regions are reversed. The largest degree of migration occurs in the higher eccentric cases and it was found that the pressure migration is independent of the test flow and rotor conditions. Finally, Winslow and Morrison found that shear stress does not contribute to conditions at the wall of the stator thereby invalidating the assumption that the axial velocity is a maximum at the maximum clearance location.

Robic (1999) experimentally and numerically measured the effect of pre-swirl on the pressure distribution in whirling annular seals. Robic found that an increase in the Reynolds number for a given Taylor number tends to reduce the effect of pre-swirl and that for negative or no pre-swirl, the overall moment tends to rotate the rotor thereby closing off the exit flow and opening the entrance on the right side of the minimum clearance.

Finally, Suyanaranyanan (2003) experimentally measured the effect of whirl ratio for a 50% smooth annular seal and experimentally measured the wall pressure distribution for a 50% eccentric annular seal for both positive and negative whirl ratios. The 'saddle back' effect noted in the research of Johnson, Thames, Das, Winslow, and Robic, was found to switch sides from the 'pressure side' to the 'suction side' at a whirl ratio of 0.8 and 0.9 for positive whirl ratios and between -0.7 to -1.0 for negative whirl ratios.

Rotordynamic Characteristics Investigations

Hori (1959) experimentally recorded and numerically calculated differences in amplitude between small and large vibrations by changing the shaft loads and compared the results to those of articles published since 1925. Hori treated oil whip as more a problem of dynamical stability of a rotor and in his numerical analysis assumed that the suction side of the journal bearing was zero, instead of negative. Hori theoretically calculated the pressure distribution within a journal bearing and found that the equilibrium position changes with increasing speed. Furthermore, Hori also discussed stability in terms of small and large rotor vibrations. Hori found that for small vibrations the rotor is always stable if the journal displacement is 80% of the radial clearance or if the vertical displacement is less than 50% of the clearance. And that for large rotor vibrations, the frequency of rotation can reach the natural frequency of the rotating shaft if the rotor speed reaches twice the critical speed. In the end, Hori found that stabilization occurs when either the eccentricity is increased (by using shorter bearings and less viscous lubricants) or when the oil force in increased (by using longer bearings or more viscous

lubricants). Hori notes that this is in direct opposition to each other but does not give his reasoning behind this occurrence.

Fritz (1970) continued upon the experiments of Hori by investigating the hydrodynamic mass and damping effects of a liquid in a thin annulus surrounding a vertically oriented rotor assembly. Data on the hydrodynamic mass, fluid damping and stability limit for synchronous whirl where computed and measured. Dynamic stability was analytically determined to be met if the rotor speed is less than twice the critical speed.

Lund and Saibel (1967) solved the nonlinear equations of the hydrodynamic force by an averaging method not previously used in journal bearing analysis. Lund and Saibel theoretically calculated the conditions for whirl to occur and explored the hypothesis that journal orbits have stable, finite bounds by analyzing a rotor supported in plain cylindrical journal bearings. And though hydrodynamic forces had been thought to contribute to rotor stabilization, Lund and Saibel found that hydrodynamic forces cannot stabilize the rotor expect in a narrow range around the threshold speed. Lund and Saibel recommend against designing above speeds where oil whip occurs, due to the erratic and uncertain nature of oil whip orbits.

Black (1969) developed a linearized theory for plain seals with inclusion of squeeze forces so that damping and stiffening actions could be estimated. Black concluded that the damping forces associated with squeeze actions are large and that for seals where the seal length to clearance ratio is large that inertial forces may cause negative stiffnesses. And that hydraulic whip instability at high speeds may result from the rotation of fluid within the seal.

Allaire et al. (1977) extended previous theories of short plain centered seals to large eccentricies and included surface roughness effects in their analysis. A "Bernoulli" effect is found to occur when the shaft is eccentric in the seal creating a hydrodynamic force in the direction opposite to the shaft eccentricity. Allaire et al. found that stiffness and damping are strong functions of eccentricity and that for high Reynolds numbers, the

Bernoulli affect becomes stronger and the load capacity increases due to the higher pressure gradients around the seal.

Childs (1983) analytically determined a way to solve for rotordynamic coefficients of high-pressure annular seals with correction coefficients for inlet swirl conditions with expression derived to refine dynamic coefficients for high-pressure annular seals and inter-stage seals used in multi-stage centrifugal pumps. Using Hirs (1973) bulk-flow equations as a basis, Childs developed rotordynamic coefficients that incorporated all of the previous developments into understanding rotordynamic coefficients for seals where small circular motions about a centered position occur. Childs' analysis was presented in two parts: first, solutions for the influence of inlet swirl with comparisons between rotordynamic coefficients derived from Hirs' model and previous results and second, a development of a finite-length solution procedure for perturbation equations. Child found that inlet swirl reduces the cross-coupled coefficients and therefore is required to obtain an accurate prediction of rotordynamic stability and response characteristics. Therefore, Childs demonstrates that the inlet swirl and inertia terms, ignored in Reynold-equation approaches, is essential for prediction of cross-coupled stiffness and direct damping terms.

EXPERIMENTAL FACILITY

The experimental facility is divided into four systems:

1. Water supply system
2. Seal-Motor Rig test section
3. Instrumentation and Computation
4. Eccentricity and whirl setting unit

Water Supply System

Water is supplied to the test section by a 10 HP ITT 734 Plus centrifugal pump (Figure A1) which is supplied by a 19m^3 tank. Water is pumped at 600±30kPa (90±2psi) to the test section and, to prevent cavitation, the upstream pressure is maintained at 138kPa (20psi). Both the supply tank and the centrifugal supply pump are located outside of the test facility; see Figure A2. The water temperature is maintained at 30.5±4°C by a 75kW heat exchanger to insure that the thermal expansion of the annular seal stays within limits. The water entering the test section is filtered twice; once by a 10μ filter and again by a wire mesh directly upstream of the seal. Similar to the centrifugal pump and water supply tank, the heat exchanger and water filter are located outside of the test facility; see Figure A3. The water flow rate is measured by a 0.25% accurate turbine flow meter which has a linear range of measurement between 1.6L/s and 14.2L/s (0.42 to 3.75 gal/s). To modify and monitor the flow rate from the control room, a Masoneilan valve was installed on the water input line; see Figure A4. Low pressure compressed air is supplied to the Masoneilan valve from a connection in the test cell. Modifications were made to the Masoneilan control aperture to assure that the desired flow rates could be attained.

Seal-Motor Rig Test Section

The seal-motor rig test section (Figure A5) can be further divided into two subsystems: the test section and the oil supply system. Each subsystem has a specific function related

to the operation of the seal-motor test rig. The oil system is used to lubricate and cool the rotor bearings while the test section is where the pressure measurements occur.

The test section is comprised of two parts: the inlet and the stator-rotor sections; see Figure A6. Water flows from the first section to the second section through a stainless steel plate where the flow is straightened before entering the test section. The rotor is mounted to an overhung shaft of 50.88mm diameter. A 37kW variable speed motor rotates the rotor to a maximum speed of 5300rpm (Figure A7) and is controlled by an Eaton Dynamatic variable frequency drive. The annular seal is attached to the rotor and has an outer diameter of 164.1mm.

The clearance, c, is 1.27mm (0.05in) and is the same for all test conditions. The seal (D=163mm, L=35.6mm) can be modified to test different eccentricities as needed. For this experiment, the eccentricity is set to 25% or 0.318mm (0.0125in) of the clearance. The annular seal is made of acrylic and has the following properties (Johnson, 1989):

Young's Modulus, $E=1.24 \times 10^{10}$ Pa

Density, $\rho=913$ kg/m^3

Ultimate Strength, $\sigma_{ult}=9.507 \times 10^{10}$ Pa

Coefficient of Thermal Expansion, $\alpha=41 \times 10^{-6}$ m/m°C

Das (1993) estimated the mechanical growth of the seal at 3600 RPM using a hoop stress analysis to be 3% of the clearance (0.0386mm) and the thermal growth to be 4% of the clearance (0.006 mm/°C) for the water temperature window (30.5±4°C).

For lubrication, synthetic grade 10W40 motor oil is supplied to the seal bearings by a ½ HP oil pump (Figure A8) which also serves as the driving mechanism behind pumping oil through a tube-in-shell heat exchanger; see Figure A9. Faucet water is used to maintain the oil temperature below 160°F. With the use of full synthetic 10W40 motor oil, adequate protection is provided to an oil temperature of 160°F. In previous experiments with this oil system, the seal rig was provided higher pressures and flow rates than were required. This caused an overpressure inside the bearing housing and subsequent leakage around the drive shaft seal. A back-pressure regulator, an optical spin gage, and a re-

routing of the oil lines reduced the supply pressure and volumetric flow rate resulting in oil leakage becoming non-existent; see Figure A10. During testing, the oil temperature exiting the bearing housing maintained an equilibrium temperature range of 110-120°F and 135-143°F during 1800 and 3600 RPM testing, respectively.

Instrumentation and Computation

For the current arrangement, ten variables are simultaneously recorded: four stator wall pressures measured by Kulite Pressure transducers, the location of the seal within the stator measured with two proximeter probes, upstream pressure and pressure drop across the seal using two Rosemont pressure transducers, and optical once per revolution sensors to measure the frequency of revolution of the rotor and whirl camshaft.

Four Kulite pressure transducers with a sensitivity ranging from 0.745mV/psig to 0.762mV/psig are mounted to brass blocks specifically designed for the purpose; see Figure A11. Each brass block has the same basic configuration with various numbers of threaded counter bored holes for the Kulite transducers to fasten. Spacing of these holes depends on each block and results in an overall picture of the pressure field as a function of downstream position (Table A1). At the base of each counter bored hole, a smaller 0.4mm-diameter pinhole tap allows the Kulite transducer to measure the pressure at each downstream position (z/L). Omni-Amp II DC-Signal Amplifiers are used to add a gain of 10 onto the DC output of the Kulite transducers (Figure A12).

Olivero-Bailey et al (1993) measured pressure fluctuations with piezoresistive pressure transducers and found that they are effective in measuring high-frequency signals, similar to frequency fluctuations found in turbulent boundary layers. Olivero-Bailey et al utilized flush mounted pinhole piezoresistive Kulite pressure transducers of diameter 0.3mm. Nunes (1993) compared results from flush mounted brass plug system and a Scani-valve pressure taps and found that the Scani-valve system is unsuitable for measuring transient wall pressure.

Two Rosemont pressure transducers are used to measure the upstream pressure and the pressure drop across the seal rig using existing pressure taps previously used with a Scani-valve system. With the addition of the Rosemont pressure transducers, the gage pressure upstream of the annular seal and a corresponding pressure drop are recorded and can be used for non-dimensionalization if necessary.

Voltage data from instrumentation devices are recorded by a 16-bit Measurement Computing PCIM-DAS1602/16 A/D converter which increased the number of simultaneously sampled channels to sixteen compared; compared to four in the previous 8-bit system. If additional amplification is necessary, the A/D converter is capable of sixteen gain combinations from 1 to 880. With the use of a commercial software code Softwire, each channel is sampled simultaneously. Softwire has a maximum channel sampling frequency of 100,000 Hz, which is divided equally among active channels. Therefore, the maximum sampling rate on each channel during measurements is approximately 9,000 Hz.

To summarize, each channel measures a specific parameter:

Channel 0: Once per revolution pickup of whirl camshaft [trigger];

Channel 1: Kulite Pressure Transducer #96;

Channel 2: Kulite Pressure Transducer #97;

Channel 3: Kulite Pressure Transducer #98;

Channel 4: Kulite Pressure Transducer #99;

Channel 5: 'Left' Proximeter Probe;

Channel 6: 'Right' Proximeter Probe;

Channel 7: Once per revolution motor pickup;

Channel 8: Dead – not used;

Channel 9: Rosemont ΔP; and

Channel 10: Rosemont P.

Ensemble averaging is used to cancel out small scale turbulence and noise in the recorded pressures (channels 1 to 4). When the Reynolds number of a flow rises above the onset

of transitional flow and reaches turbulent flow, pressure measurements become unstable and fluctuate about a mean value. With the use of MatLab, over 300,000 samples per channel can be averaged and analyzed. The only limiting function is the amount of cache memory available, the processor speed, and the available time for data processing.

Eccentricity and Whirl Setting Unit

The test-rig at the Turbomachinery Laboratory was developed and built by Johnson (1989) first to measure the flow field within annular seals with a 3-D LDA system and was then was modified by Winslow (1994) to measure dynamic wall-pressure and shear stress distributions on the stator wall. Suryanarayanan (2003) modified the facility to allow the stator to orbit at various whirl ratios; see Figure A13. The eccentricity and whirl setting unit is made up of the following components (the number in parenthesis is the number of these components necessary):

- Whirl Shaft (2)
- Whirl Camshaft (2)
- Pillow Block (2)
- Whirl Camshaft Housing (2)
- Modified Stator (1)
- Modified Housing (1)
- Plunger (2)

AutoCAD drawings for the components of the eccentricity and whirl setting unit can be found in Appendix D (Figures D1-8)

The major change made to the facility between the works of Johnson and Winslow was the removal of the quartz viewing window. Four brass blocks were constructed to fit within the trapezoidal "viewing" window and were machined to allow for the use of flush-mounted piezeoresistive pressure transducers (Kulites). Each of the four blocks can be oriented in two ways, top up (Top) and bottom up (Bottom). This allows for greater coverage of the stator wall, because only four downstream pressure tap measurements can be made at one time.

A Scanivalve system was also installed which was used by Suryanranan (2003). The three major changes made to the seal test section after the work of Suryanarayanan are listed below:

- Exclusive use of piezoresistive pressure transducers
- Implementation of two proximeter probes to monitor seal eccentricity and whirl orbit
- Exchange of a 16-bit sixteen-channel A/D Converter for the previous 8-bit four-channel converter used by Suryanarayanan, Winslow, and Robic
- Development of MatLab programs to process raw data.

EXPERIMENTAL PROCEDURE

The experimental procedure can be divided into two steps: measurement and computation. The computational step can be completed during measurements or after measurements have been completed.

Measurements

The Kulite pressure transducers are calibrated with a pneumatic dead weight tester. The flow rate is set within 4.86±0.5 l/s for flow rates corresponding to Re=24000 (149.6 Hz) and 12000 (74.8 Hz). Water temperature must be maintained at 30.5±4 C (86.7±7°F) to maintain a constant Reynolds number, seal clearance, water density and water viscosity among all test runs of similar conditions. A 75kW (0.256 MMBtu/hr) heat exchanger outside the test-cell facility is used when necessary to keep the water temperature within limits. The seal is set for 25% eccentricity using the procedure set forth by Suryanarayanan (2003). A circular orbit is maintained if the phase between the two cams is 90 degrees. This orbit can be confirmed with the two proximeter probes. There are two whirl pulleys that are used; a 1:1 pulley for whirl ratios of 0 to 1.0 for 1800RPM and 0 to 0.5 for 3600RPM and a 2:1 pulley for whirl ratios of 0.6 to 1.0 for 3600RPM. It is recommended that all data runs be completed for one pulley ratio before another is put into place. The whirl ratio can be set by modifying the whirl motor speed. A brass block is placed into the test section and secured with four brass screws. The Kulite pressure transducers are screwed into the counter bored holes of the brass block and are used to measure the instantaneous wall pressures at specific downstream locations. This procedure is repeated for each of the seven block orientations, two flow rates, and two rotor speeds.

To eliminate trapped air within the seal-rig, the Kulite transducers must be bled of air before runs can commence. The main chamber of the seal-rig is also bled of air. Air must be bled from the seal-rig EVERY time the chamber is emptied of water or when

measurements continue after the test rig has been shutdown for an extended period of time. Safety against cavitation occurs when the pressure within the test-rig is above 138kPa (20psi).

The goal of this experiment is to obtain mean pressure readings and phase-averaged wall pressure readings for each downstream axial position. Rotordynamic coefficients are obtained by integrating the phase-averaged pressure distributions and plotting the results as a function of whirl ratio.

Computations

Phase Averaged Wall-Pressure Distributions

Ensemble, or phase, averaging is used to cancel out small scale turbulence and noise of instantaneous pressure measurements. The turbulence within the annular seal is a consequence of transitional flow. Pressure measurements made at the wall fluctuate about a mean value. The purpose of phase averaging is to rid the wall pressure data of turbulent fluctuations so that only the mean pressure at the wall is used for analysis. In the case of rotating components, phase averaging can calculate the mean pressure at specific rotor angular positions around the circumference of the seal with the use of a trigger. For this experiment, the trigger is a once per revolution optical gage (Channel 0). A peak in voltage from the once per revolution channel is used as the trigger to start phase averaging. This insures that similar points around the circumference are compared and averaged.

Data is saved (or transferred) to a computer with MatLab installed. The experimenter must then determine if the data is static or dynamic in nature. Dynamic whirl occurs when the whirl motor and pulley system are responsible for movement of the camshaft. Static whirl occurs when the whirl motor and pulley system are not used for movement and the operator must move the camshaft by hand. It is possible to have upwards of 360 (1 sample per degree) different data files for one condition of rotor speed, flow rate, and

block orientation when measuring static whirl but for the case of this experiment only 72 data points (1 sample per 5 degrees) were taken around the seal circumference.

When computation is necessary, MatLab is used to process the raw data into manageable forms for Tecplot. MatLab m-files are utilized for programming code to calculate values from calibration data, organize the raw data into phase cycles, and finally output text files which are plotted in Tecplot. Before beginning any data processing, it is important to insure that the proper directories are referenced within the MatLab m-files; otherwise, the program will not yield any results. It is useful to keep all raw data in a single folder that can be referenced as the current directory (cd 'directory'). If no current directory is given, MatLab looks for files to load in the directory that the MatLab program is saved. Files from this experiment were saved within two directories: E:\3600data and E:\1800data for 3600RPM and 1800RPM data sets, respectively. Additional folders contained within these directories further divides the data into an organized matrix, but it is not necessary to divide raw data for proper functionality. All that is necessary is to insure that MatLab 'looks' in the right place to find the raw data.

MatLab offers a wide range of toolboxes and commands that assist in programming for engineering and mathematical purposes. The most useful purpose of MatLab is that mathematical programs and subroutines can be written easily for a variety of data calculations. In this experiment, MatLab is used to:

1. Identify cycles and count the number of samples per cycle

2. Organize data into matrices by which phase averaging can occur

3. Calculate pressures and positions with use of calibration equations

4. Calculate the phase averaged wall-pressure distributions, mean downstream pressures, and component forces of the seal

5. Collect data into text files which can be plotted with Tecplot

Contours.m is modified to include desired text files to be ensemble averaged for conditions of dynamic whirl. Contours.m is comprised of two internal programs, Cycles.m and Values.m, which should be checked for consistency before computing results. Cycles.m is a subroutine which uses a trigger (Channel 0) to divide the text file into cycles to be phase averaged. Values.m is a subroutine which takes values from Cycles.m and applies the calibration numbers to the voltage data and defines additional variables for the Sommerfeld Journal Coeffficients. Values.m should be checked for consitency with calibration equations before running; however as of this time multiple calibration curves cannot be supported. Only one set of calibration numbers for each port is supported at this time. Users should also check the Sommerfeld Journal Bearing equation constants to ensure that the proper radius, clearance, viscosity, and rotor speed will be used in the calculation of the pressure coefficient (C_p). Each file is loaded into the MatLab workspace by Contours.m where the Cycles.m and Values.m subroutines are carried out. Then all the data for each test run is saved separately as a MatLab workspace file (.mat) so that data for mean pressures, positions, and percentage cycle can be loaded for future calculations. Finally, Individuals.m outputs text files for each condition of dynamic whirl, so that a Tecplot carpet plot can be created; however Individuals.m must be modified to load MatLab workspace files (.mat) for particular whirl frequencies and flow rates. In other words, Individuals.m tabulates and saves variables from each block orientation for a specific whirl ratio, flow rate, rotor speed combination. For example, when all the data for Re=24000, Ta=3300, and β=0.3 have been collected from the seven block orientations; Individuals.m is used to collect the data from each test run. In all, there are 40 different combinations (Figures B1-40) for dynamic whirl.

Rotordynamic Coefficients

The rotordynamic coefficients are calculated for each operating condition by curve fitting the equations defined by Childs (1983) with the x- and y-component forces on the rotor seal. The component forces are found by integrating the phase averaged pressure distributions. Coefficient1.m and Coefficients2.m are used in conjunction with Rotor.m to determine the relevant data for each port, find the component force per unit circumference, then find the overall component forces with data for the downstream

positions.   Integration for the rotordynamic coefficients it not a full integration but instead is a summation of the components of the pressures about the seal.   The numbers which MatLab calculates are input into Excel where the forces are formatted to fit within the parameters defined by Childs.

RESULTS AND DISCUSSION

Phase Averaged Wall-Pressure Distributions

The classical equation for journal bearings is the Sommerfeld equation. For the purposes of comparison, a non-dimensional pressure coefficient in the form of Sommerfelds' classic equation is used.

$$C_P = \frac{P^* c^2}{6 \mu \omega R^2}$$

The difference between the phase averaged pressure and overall mean pressure characterizes the amount of deviation of each point around the circumference of the seal from the mean pressure at each downstream position.

$$P^* = P - \overline{P}$$

Each circumferential position has a particular value for P^* from the formula above. First, the mean pressure $\left(\overline{P}\right)$ for each axial position is calculated by taking the mean of all the data taken by each Kulite pressure transducer at the specified running conditions. Then, MatLab calculates the phase averaged pressure (P) for each circumferential position at each axial position. P^* is then calculated as the difference of the phase averaged pressure and the mean pressure which account for deviations from the mean pressure at each circumferential position.

Rotordynamic Coefficients

The procedure for calculating the rotordynamic coefficients for each rotor speed and flow rate combination is outlined in Childs' (1983) analysis of turbulent seals and is based on Hirs' Lubrication Equation. The phase averaged pressure distribution at discrete points along the seals' circumference and downstream seal position are measured, so the forces on the rotor in the x- and y-directions (origin at rotor/stator center when eccentricity is zero) are calculated by evaluating:

$$\vec{F} = -\int p \, d\vec{A}$$

The x- and y-components of the force on the rotor can therefore be calculated using:

$$F_x = -\int_0^{2\pi}\int_0^1 p \cos\theta \, dZ \, Rd\theta$$

$$F_y = -\int_0^{2\pi}\int_0^1 p \sin\theta \, dZ \, Rd\theta$$

The seal geometry dictates the bounds of the integration to find the component forces. Since the pressure data are recorded at discrete spatial locations, the integrals become summations of equal arc length of the circumference and equal divisions of the distances between pressure tap locations.

$$F_x = -\sum_{j=1}^{m}\frac{1}{2}RL\pi\left(\sum_{i=1}^{n}p_i\cos(2\pi C_i)*(C_{i+1}-C_{i-1})\right)_j\left(\Delta\left(Z/L\right)_{j-1\to j}+\Delta\left(Z/L\right)_{j\to j+1}\right)$$

$$F_y = -\sum_{j=1}^{m}\frac{1}{2}RL\pi\left(\sum_{i=1}^{n}p_i\sin(2\pi C_i)*(C_{i+1}-C_{i-1})\right)_j\left(\Delta\left(Z/L\right)_{j-1\to j}+\Delta\left(Z/L\right)_{j\to j+1}\right)$$

The rotordynamic coefficients $\left(\widetilde{K}, \widetilde{k}, \widetilde{C}, \widetilde{c}, \widetilde{M}, \widetilde{m}\right)$ are calculated by plotting the coefficients of force (right-hand side of the following equations) with respect to whirl ratio and finding the least squared curve fit:

$$-\frac{\lambda F_x(\Omega T)}{\pi R\Delta P R_o} = \widetilde{K} + \widetilde{c}(\Omega T) - \widetilde{M}(\Omega T)^2$$

$$\frac{\lambda F_y(\Omega T)}{\pi R\Delta P R_o} = \widetilde{k} - \widetilde{C}(\Omega T) - \widetilde{m}(\Omega T)^2$$

The friction-loss coefficient (λ) in the previous equations is defined as:

$$\lambda = n_o\left(\frac{\rho Vc}{\mu}\right)^{m_o}\left[1+\frac{1}{4}\left(\frac{R\omega}{V}\right)^2\right]^{\left(1-m_0/2\right)}$$

But can be reduced to available variables:

$$\lambda = n_o(\mathrm{Re})^{m_o}\left[1+\frac{1}{4}\left(\frac{2R^2c\pi\omega}{Q}\right)^2\right]^{\left(1-m_o/2\right)}$$

Effects of Whirl Ratio, Taylor Number, and Reynolds Number on the Phase Averaged Pressure Distributions

The contour plots for the phase averaged wall-pressure distributions for Ta=3300 and Ta=6600 are discussed in the following section. Whirl ratios of 0.1 to 1.0 were measured for flow rates corresponding to Re=24000 and Re=12000 and an eccentricity ratio of 25%. Previous research by Johnson, Robic, and Suryanarayanan tested 50% eccentricity but comparisons will be made to their measurements. Positive whirl occurs when the rotor and seal rotate in the same direction. The contours are presented as functions of the Coefficient of Pressure (C_p) which is derived as a variation of the Sommerfeld Journal Bearing equation. The remaining axes, shown as % cycle and z/L, represent the percentage cycle and normalized downstream position for the annular seal; where 0% cycle represents the maximum clearance location and 50% cycle represents the minimum clearance location. The "pressure" side of the seal occurs within the range of 0-50% cycle as the clearance decreases and the mean pressures increase along the circumference of the seal. The "suction" side of the seal occurs within the range of 50-100% cycle as the clearance increases and the mean pressures decrease along the circumference of the seal. The phase averaged wall-pressure distributions aid in understanding the complex fluid motions within the seal. All flow conditions were conducted with zero pre-swirl.

Ta=3300, Re=24000, ε=25%, β=0.1 to 1.0

Figures B1-19 (odd) show the phase averaged wall-pressure distributions for a rotor speed of 1800RPM and a flow rate of 4.86 L/s; corresponding to a Ta=3300 and a Re=24000. Similar flow conditions were reported by Suryanarayanan (2003) but for ε=50%. When the whirl ratio is 0.1, the pressure distribution is marked by azimuthial pressure bands axially spaced z/L=0.175 apart with measured pressures ranging from ±2.5. The pressure bands continue to grow in size and remain equally spaced axially as the whirl ratio increases to 0.8. When the whirl ratio reaches 0.8 the pressure bands lose dominance to axial striations. San Andrés (2000) notes that centrifugal instabilities similar to that recorded are characterized by Taylor-Gortler vortices in which circular flows perpendicular to the transit velocity occur within the flow annulus. It is hypothesized that for β>0.7, the average circumferential velocity, and circumferential

Reynolds number, increases due to the inner rotor pushing fluid particles which effectively increase the Taylor number above the Taylor-Gortler instability range. Flow disturbances similar to the measured azimuthial pressure bands were recorded by Suryanarayanan. Increasing whirl caused the vortices to disappear for β=0.2, however reappear at β=0.3. When the vortices reappear at a whirl ratio of 0.3 the number of pressure disturbances decreases axially as the vortices grow and move about the circumference of the seal. The azimuthal movement of the vortices at β=0.3 shows that the whirling of the seal begins to effect the downstream motion of the fluid and that circulation might be occurring along the circumference of the seal. As the whirl ratio increases above 0.3, the size of the vortices continues to increase and move about the circumference of the seal. San Andrés notes that Taylor-Gortler vortices are functions of the Taylor number and Reynolds number; however it appears that the whirl ratio does have an affect. The switch in pressure distribution at the seal exit appears to occur above β=0.7, which is similar to that reported by Suryanarayanan (2003) and Robic (1999). The maximum variation in pressure occurs when β>0.7 and ranges between ±3. When the whirl ratio reaches 0.9, axial striations begin to emerge along the 50% cycle position. These might be a manifestation of the phenomenon measured by Robic which were attributed to longitudinal vortices and conical motions about the seal center.

Table B1 shows the axial pressure drop across the seal for conditions of whirl from 0.1-1.0 for Ta=3300 and Re=24000. The disappearance of the azimuthial pressure bands at β=0.2 is accompanied by a 4% increase in the pressure drop across the seal from β=0.1. When the azimuthial pressure bands return at β=0.3 the pressure drop decreases by 8% from β=0.2. The axial pressure difference remains stable until the switch in the pressure distribution occurs at β=0.8 at which point the pressure difference increases by 7%. With further increases in the whirl ratio the axial pressure difference continues to increase. It appears that the azimuthial pressure bands act to lower the pressure drop while more developed flow conditions seen at whirl ratios greater than β=0.8 act to increase the seal pressure drop.

Figure B41 shows the seal orbit for Ta=3300 and Re=24000. The orbit follows a similar path for whirl ratios 0.1-1.0 ranging between ±0.01in but the orbits do not match up exactly. From the graph, it appears that the orbits begin to change as the whirl ratio increases from 0.1 to 1.0. This might be due to an inertial effect of the modified stator (Figure D6) and plunger (Figure D8).

Ta=3300, Re=12000, ε=25%, β=0.1 to 1.0

Figures B2-20 (even) show the phase averaged wall-pressure distributions for a rotor speed of 1800RPM and a flow rate of 2.43 L/s; corresponding to Ta=3300 and a Re=12000. The pressure distributions for the Re=12000 case are very similar in structure to that of the Re=24000 case; however the azimuthial pressure bands so prevalent in Figures B1-19 (odd) are not as pronounced. Taylor-Gortler vortices are already known to be functions of the Reynolds and Taylor number; however, as previously mentioned the whirl ratio has a significant affect. The pressure distributions remain relatively constant until the pressure distribution flips at β=0.7 (Figure B14), at which point the pressure distribution for the Re=12000 case looks almost identical to that of the Re=24000 case expect for the difference in magnitude. Peak pressure measured ranges between ±1.5 for all whirl ratios. The axial striations noticed in the Re=24000 case are more prevalent in the Re=12000 case. As the whirl ratio increases from 0.9 and 1.0 the region of maximum pressure begins to grow along the entire axial length of the seal about the location of minimum clearance. The Taylor-Reynolds effect mentioned by San Andrés accounts for the dynamic appearance of these striations at Re=12000. When the Reynolds number is low there is less flow energy to flush pressure disturbances from the seal annulus. Similar striations can be seen in the low pressure region between z/L=0.6 and 1.0. It appears as if the striations measured are similar to a breaking wave pattern seen on free surfaces where the fluid within the seal is being pushed azimuthally by the inner cylinder faster than it can transit through the seal axially.   When considering the plots for Ta=3300, Ra=12000 and Re=24000, it appears that there might be a quantifiable number made up of the Taylor number and the whirl ratio which characterizes the appearance of these pressure bands.   The Reynolds number seems to have only an effect on the magnitude of the pressure striations (Figures B19 and B20).

The axial pressure differences for Ta=3300 and Re=12000 can be found in Table B1 of Appendix B. The relatively constant pressure distributions for whirl ratios 0.1-0.7 leads to mean pressure distributions which do not fluctuate more than 5%. When the appearance of axial striations is measured at β=0.8, the axial pressure difference increases by 10% from β=0.7. Further increases in the whirl ratio lead to increases of 16% and 11% for β=0.9 and β=1.0, respectively. For the case of Re=12000 mean pressure differences range between 56-65% less than that of similar whirl ratios for Re=24000.

Figure B42 shows the whirl orbit for Ta=3300 and Re=12000. The orbit for the seal is relatively constant with some deviation by the whirl cases higher than β=0.7. The orbits for the Re=12000 are very similar in size and character to the orbits for Re=24000.

Ta=6600, Re=24000, ε=25%, β=0.1 to 1.0

Figures B21-B39 (odd) show the phase averaged wall-pressure distributions for a rotor speed of 3600RPM and a flow rate corresponding to a Re=24000 and Ta=6600. The major difference between the plots of Re=24000 and Re=12000 for Ta=6600 is the difference in magnitude. The azimuthial pressure bands observed in the Ta=3300 (1800RPM) case is not as pronounced for the Ta=6600 cases. The Taylor-Gortler vortices do not appear in Figures B21-B39 (odd), probably due to the fact that the Taylor number is above the range where these vortices occur. The phase averaged wall-pressure measurements are relatively uniform until a whirl ratio of 0.4; indicating minimal forces exerted by the fluid upon the rotor. At β=0.5, the axial pressure striations noted by Robic to be longitudinal pressure bands begin to emerge. These bands grow in magnitude as the whirl ratio increases to 1.0 while it appears that the bands migrate from 60% cycle to 30% cycle as the whirl ratio is increased from β=0.5 to β=1.0. A large pressure region at 80% for β=0.7 which grows and ebbs as the whirl ratio increases to β=1.0 appears to be multiple stacked pressure striations. In other words, the high pressure region at β=1.0 is constructed of overlapping axial striations. A low pressure region of similar axial and azimuthial size was also recorded 50% cycle ahead of each high pressure region. The low pressure regions are suction zones where the inner cylinder pulls on fluid particles.

However, the low pressure regions are not characterized by pressure striations. The maximum pressure differences occur when the whirl ratio reaches 0.7. At this point, the measured pressures range around ±6. The switch in pressure between the seal inlet and exit occurs above β=0.5. This is similar to the measurements of Suryanarayanan; however the research for Suryanarayanan stops at a whirl ratio of 0.5.

The axial pressure drop can be found in Table B1 for Ta=6600 and Re=24000. The lack of azimuthial pressure bands again acts to decrease fluctuations in the seal pressure drop to less than 1% for whirl ratios below 0.5. Upon the emergence of axial pressure striations, the pressure drop increases by 8% and continues to increase by approximately 10% for each increase of 0.1 in whirl ratio. Similar to the cases of Re=24000 and Re=12000 for Ta=3300, the appearance of axial pressure striations increases the measured pressure differential across the seal and the growth of the axial striations accompanies a further increase in the seal pressure drop. When the whirl ratio reaches 1.0, however, the pressure difference across the seal drops by 12% from β=0.9 as the regions of high and low pressure dissipate and decrease in size by approximately 50% which could be a function of the orbit change of the seal.

The seal orbit is presented in Figure B43 for Ta=6600 and Re=24000. Previous research with this set-up, conducted by Suryanarayanan, only measured flow fields for whirl ratios up to β=0.5 for Ta=6600. The measurements for β>0.6 are new with this test set-up and it appears that the whirl and eccentricity setting unit encounters problems when measuring flow fields of high whirl ratios. The orbit becomes large and disfigured when compared to that of β≤0.5. As mentioned previously, this might be an effect of inertial forces of the modified stator or could be the tension belt stretching and changing the phase between the plungers. The static eccentricities were checked to verify that the mechanical components had not slipped. Therefore, the orbit variation is due to the dynamics of the shaker mechanism, the flow field, or a combination of the two. The irregular orbits might also be a manifestation of the phase averaging method. For the cases of Ta=3300, the seal is traveling at a velocity in which the seal position measured is very similar for each point around the circumference. Figure B43 shows that the whirl

orbit up to β=0.5 is regular and elliptical like that of Ta=3300 for Ta=6600. However, when the whirl ratio increases to 0.6, the measured seal positions are not similar around the circumference. Therefore, a more discreet set of data is being phase averaged. In other words, when the Taylor number is low the seal is traveling about the seal slow enough that when measurements are taken at each position around the seal circumference similar values for the seal position are being measured for each cycle of the phase averaging. When the Taylor number increases to 6600 and the whirl ratio is greater than 0.5, the measured seal position for each cycle of the phase average is more random and therefore a larger deviation between cycles for the seal position is measured. These deviations in seal position, when averaged, give an orbit that is not similar to that of Ta=3300.

Ta=6600, Re=12000, ε=25%, β=0.1 to 1.0

Figures B22-40 (even) show the phase averaged pressure distribution for Re=12000 for the case of 3600RPM. When looking at the plots as a whole it is noticed again that the only difference between the Re=24000 and Re=12000 cases is a difference in magnitude. Large regions of high and low pressure at the seal exit are recorded. These regions grow in magnitude and circumferential size as the whirl ratio increases from 0.2 to 0.5. The axial striations observed in the Ta=3300 case for Re=12000 start to emerge at a whirl ratio of 0.5, but dissipate at a whirl ratio of 0.6. These striations appear again as the whirl ratio increases to 0.7 and continue to grow along the axial length of the seal as the whirl ratio increases to 1.0. In contrast to Ta=3300, the striations do not remain at the same position on the seal throughout their appearances; instead migrate from a position of 55% cycle to 35-40% cycle as the whirl ratio increases above 0.6. However, in the case of Ta=6600 the axial pressure bands begin to drift apart as the whirl ratio increases to 1.0. This affect is more noticeable for the Re=12000 case than for the Re=24000 case. The switch in the pressure and suction zones occurs earlier for the Ta=6600 cases as the regions of high and low pressure begin migrating about the circumference of the seal at lower relative whirl ratios. When the whirl ratio reaches 0.5, the switch of the pressure side and suction side is completed and remains as the whirl ratio continues to increase to 1.0.

Values for the axial pressure drop across the seal is tabulated in Table B1 for Ta=6600 and Re=12000. Similar to the case of Re=24000 and Ta=6600, the axial pressure drop remains constant throughout the range of whirl ratios 0.1-0.3. Upon the appearance of axial striations, the axial pressure distribution increases by 17% as the whirl ratio increases from 0.3 to 0.4. An increase of 43% occurs in the seal pressure drop at β=0.7 which is followed by a 37% decrease. And as the whirl ratio increases from 0.8 to 1.0 the pressure drop continues to increase and decrease by 39% and 18%, respectively. Similar to Ta=6600 and Re=24000, the seal pressure difference drop decreases as regions of high and low pressure decrease in size by approximately 50% when the whirl ratio increases from 0.9 to 1.0.

Figure B44 shows the seal orbit for Ta=6600 and Re=12000. The orbits for Re=12000 are similar to that of Re=24000 for Ta=6600. The orbits start tight and uniform up to a whirl ratio of 0.5 after which the orbit changes significantly. This is the first time that whirl orbits were measured with a proximeter probe and it appears that β=0.5 is the upper limit for consistent whirl orbits without modifications to the eccentricity and whirl setting unit.

The pressure contours vary in magnitude for Ta=3300 and Ta=6600 between ±3 and ±6, respectively. The greatest pressure measurements occur when the whirl ratio is 1.0 for all Taylor number and Reynolds number combinations. The largest pressure contour occurs when the Taylor Reynolds ratio is 3.63 for Ta=6600 and 7.273 for Ta=3300 or when the Reynolds number is 24000 for β=1.0.

Effects on Childs Rotordynamic Coefficients' due to Reynolds Number and Taylor Number

The least squared fit for the rotordynamic coefficients varied depending on the calculated force coefficient and the operating conditions. Most curve fits had correlation coefficients greater than 0.6, however the curve fits for conditions relating to the x-component force for Ta=3300 Re=24000 and Ta=6600 Re=12000 as well as the

condition relating to the y-component force for Ta=3300 Re=12000 did not. Overall, the calculated forces were random up to $\beta<0.5$ due to wall-pressure distributions which are relatively flat and have no defined structure (Figures C1-C7 odd). The procedure defined by Childs (1983) to determine the rotordynamic coefficients is only valid for small circular motions about the seal center and in the case of this experiment, the whirl orbits are neither. The seal orbits are elliptical for all test cases (Figures B41-B44) with large oscillations in the whirl orbit at Ta=6600 (Figures B43 and B44) most prevalent when the whirl ratio increases above 0.5. Due to the non-circular orbit, Childs (1983) analysis cannot be used to find the rotordynamic coefficients at this time. Steps must be taken to ensure that the measured pressure field occurs within a whirling seal where small oscillations occur about the seal center; otherwise Childs analysis is not valid and will not obtain meaningful results.

CONCLUSION

This work presents an effort to explore the effect of whirl ratio, Taylor number, and Reynolds number on the phase averaged wall-pressure distributions and rotordynamic coefficients for a 25% eccentric whirling annular seal. The test section was designed first for stationary flow conditions then further modified to simulate fractional whirl ratios. Testing was performed at Re=24000 and Re=12000 for Ta=3300 and Ta=6600. Positive whirl ratios (0-1.0) were tested. Measurements were made by piezoresistive pressure transducers and the results were calculated by MatLab.

Figures B1-B40 show the phase averaged wall-pressure distributions for Ta=3300 and Ta=6600. Two flow rates were measured for whirl ratios 0.1-1.0. The phase averaged wall-pressure distribution for Ta=3300 and Re=24000 show signs of Taylor-Gortler vortices from a whirl ratio of 0.1 to 0.7. The vortices grow in size and azimuthally move around the seal with increasing whirl ratio. When the whirl ratio reaches a point where the annular seal is rotating at 1800RPM, the Taylor-Gortler vortices disappear and longitudinal vortices appear in the pressure distribution. It is believed that the whirl ratio and flow rate plays a role in determining the appearance of Taylor-Gortler vortices or longitudinal vortices and can be quantified as combination of the Taylor number, whirl ratio and Reynolds number. The maximum pressures measured for Ta=3300 occurs at a whirl ratio of 1.0 for both Re=24000 and Re=12000; ±3 and ±1.5, respectively.

The phase averaged wall-pressures for Ta=6600 did not yield measurements of Taylor-Gortler vortices for whirl ratios 0-0.4 which were as pronounced as in the Ta=3300 case, however the appearance of longitudinal vortices did appear at β=0.5, or when the whirl speed reached 1800RPM. The longitudinal vortices moved about the seal as the whirl ratio increased further; changing azimuthally by 30-35% of a cycle. The pressure distributions showed the same dependence on Reynolds number where the pressure fluctuations for Re=12000 and Re=24000 were exactly half of each other; ranging from ±3 and ±1.5 for β≤0.4 and ±6 and ±3 for Re=24000 and Re=12000, respectively. The

"switch" in the pressure distribution whereby the pressure and suction sides of the seal flip from the seal entrance to seal exit occurred at $\beta=0.7$ for Ta=3300 and $\beta=0.4$ for Ta=6600, this concurred with previous investigations.

Future investigations should be focused towards determining the best way to obtain reliable fits for the rotordynamic coefficients including analysis for non-circular orbits and how to obtain circular orbits in the test facility. The mechanisms behind Taylor-Gortler and longitudinal vortices can also be investigated for whirling annular seals through CFD modeling of the seal annulus and measurements of the wall-pressure distributions for additional Taylor numbers and Reynolds number combinations. Simulations can aide in determining the role of Taylor number, Reynolds number, and whirl ratio in the appearance of Taylor-Gortler and longitudinal vortices without the high cost of physical experimentation. Finally, determining a way to use programs developed in MatLab to instantaneously plot the normalized mean pressure distributions, phase averaged wall-pressure distributions and rotordynamic coefficients would be a challenging goal for future study.

REFERENCES

Allaire, P. E., Lee, C. C., and Gunter, E. J., 1977, "Dynamics of Short Eccentric Plain Seals with High Axial Reynolds Number," *Journal of Spacecraft and Rockets*, Vol. 15, pp. 341-347.

Black, H. F., 1969, "Effects of Hydraulic Forces in Annular Pressure Seals on the Vibrations of Centrifugal Pump Rotors," *Journal of Mechanical Engineering Science*, Vol. 11, No. 2, pp 206-213.

Brennen, C., 1976, "On the Flow in an Annulus Surrounding a Whirling Cylinder," *Journal of Fluid Mechanics*, Vol. 75, No. 1, pp. 173-191.

Childs, D. W., 1983, "Finite-Length Solutions for Rotordynamic Coefficients of Turbulent Annular Seals," ASME *Journal of Lubrication Technology*, Vol. 105, pp. 429-436.

Das, P. G., 1993, "3-D Laser Doppler Velocimetry Measurements of Eccentric Annular and Labyrinth Seals," M.S. Thesis, Texas A&M University, College Station.

DiPrima, R. C., Stuart, J. T., 1972, "Flow Between Eccentric Rotating Cylinders," ASME *Journal of Lubrication Technology*, Vol. 94, pp. 266-274.

Fritz, R. J., 1970, "The Affects of an Annular Fluid on the Vibrations of a Long Rotor," ASME *Journal of Basic Engineering*, Vol. 92, pp. 923-937.

Hirs, G. G., 1973, "A Bulk Flow Theory for Turbulence in Lubricant Films," *Journal of Lubrication Technology*, Vol. 95, pp. 137-146.

Hori, Y., 1959, "A Theory of Oil Whip," ASME *Journal of Applied Mechanics*, Vol. 26, pp. 189-198.

Johnson, M. C., 1989, "Development of a 3-D Laser Doppler Anemometry System: With Measurements in Annular and Labyrinth Seals," Ph.D. Dissertation, Texas A&M University, College Station.

Lund, J. W., Saibel, E., 1967, "Oil Whip Whirl Orbits of a Rotor in Sleve Bearings," ASME *Journal of Engineering for Industry*, Vol. 89, pp. 813-823.

Morrison, G. L, DeOtte, R. E., and Thames, H. D., 1994, "Experimental Study of the Flow Field Inside a Whirling Annular Seal," *STLE Tribology Transactions*, Vol. 37, pp. 425-429.

Morrison, G. L., and Winslow, R. B., 1995, "Forces and Moments Generated by Pressure and Shear Stresses on the Stator of a Whirling Eccentric Seal," *31st Joint Propulsion Conference and Exhibit*, San Diego, California, AIAA 95-2766.

Newkirk, B. L, and Taylor, H. D., 1925, "Shaft Whipping Due to Oil Action in Journal Bearings," *General Electric Review*, Vol. 28, pp. 985-988.

Nunes, S. J., 1993, "A Comparison of Pressure Measurement Systems for an Annular Seal with Whirl," Senior Honor's Thesis, Department of Mechanical Engineering, Texas A&M University, College Station.

Olivero-Bailey, P., Forestier, B. E., Focquenoy, E., and Olivero, P., 1993, "Wall-Pressure Fluctuations in Natural and Manipulated Turbulent Boundary Layers in Air and Water," ASME FED-.168, *Flow Noise Modeling, Measurement, and Control*, Winter Annual Meeting, New Orleans, Louisiana, pp. 63-74.

Robic, B. F., 1999, "Experimental and Numerical Analysis of the Effect of Swirl on the Pressure Field in Whirling Annular and Labyrinth Seals," Ph.D. Dissertation, Texas A&M University, College Station.

San Andrés, L. A., 2000, *Turbulence in Thin Film Flows*, Distributed in MEEN 626, Texas A&M University, College Station.

Suryanarayanan, A., 2003, "Experimental Measurement and Analysis of Wall Pressure Distribution for a 50% Eccentric Whirling Annular Seal," M.S. Thesis, Texas A&M University, College Station.

Thames, H. D., 1992, "Mean Flow and Turbulence Characteristics in Whirling Annular Seals," M.S. Thesis, Texas A&M University, College Station.

Winslow, R. W., 1994, "Dynamic Pressure and Shear Stress Measurements on the Stator Wall of Whirling Annular Seals," M.S. Thesis, Texas A&M University, College Station.

APPENDICES

APPENDIX A

TEST SECTION DIAGRAMS AND PHOTOS OF TEST FACILITY
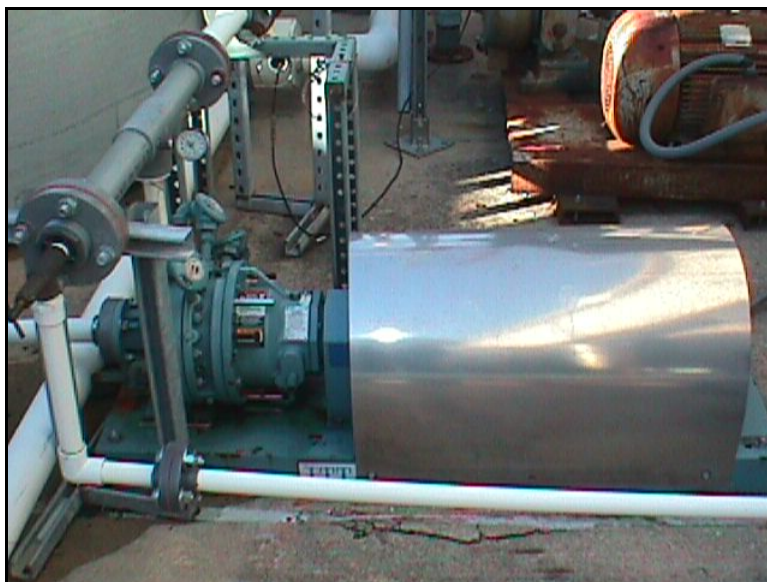
Figure A1: ITT 734 Plus Centrifugal Pump with Protective Shielding

Figure A2: Supply Tank, Water Filter, and Centrifugal Pump

Figure A3: Heat Exchanger and Water Filter

Figure A4: Masonelian Valve
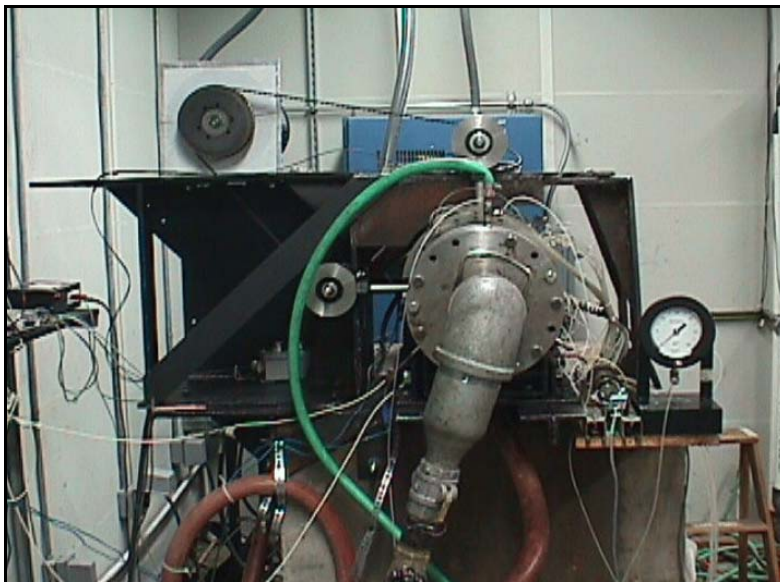
Figure A5: Overall Exterior View of Seal Rig Test Section
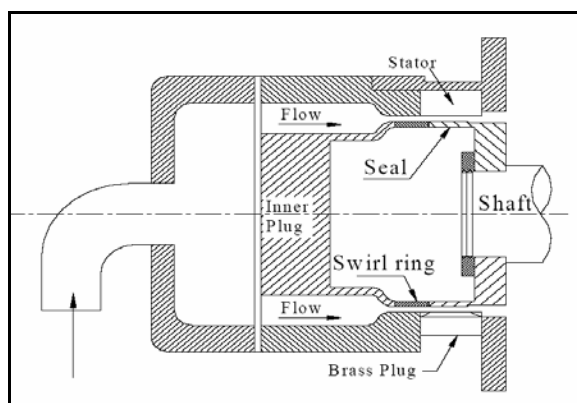
Figure A6: Cross Sectional View of Seal Test-Rig

Figure A7: Seal Rig Motor
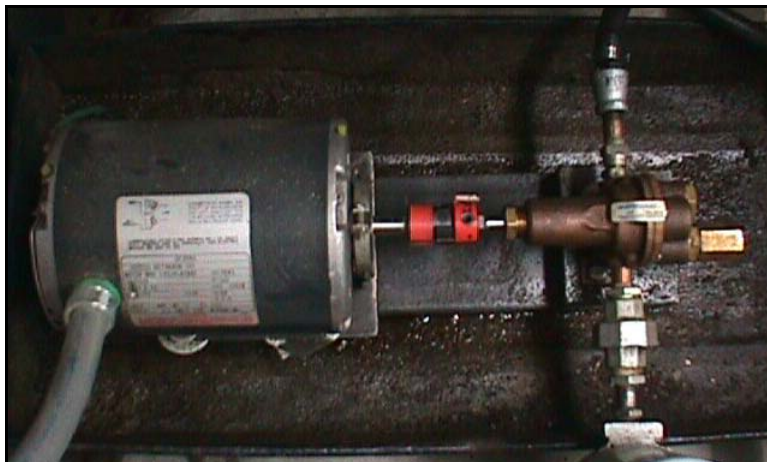
Figure A8: 1/2 HP Oil Circulation Pump
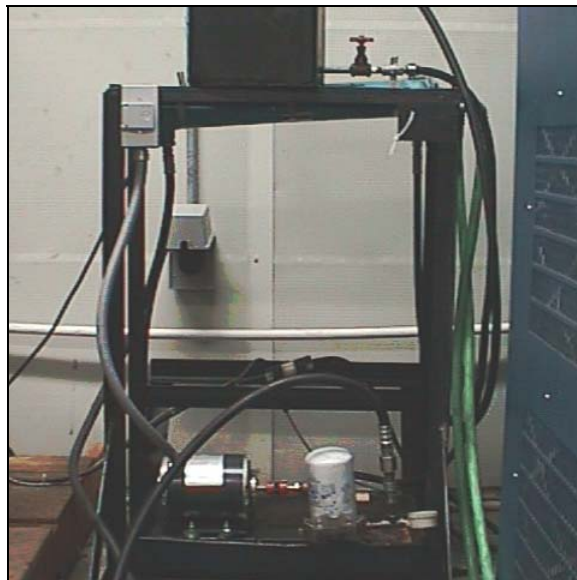
Figure A9: Oil Cooling and Circulation System

Figure A10: Back-Pressure Regulator and Optical Spin Gauge
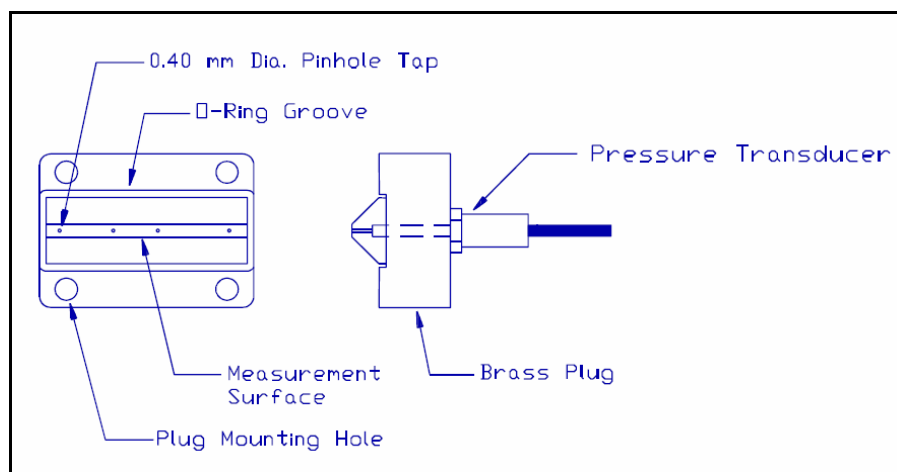
Figure A11: Piezoresistive Pressure Transducer Mounting Brass Block
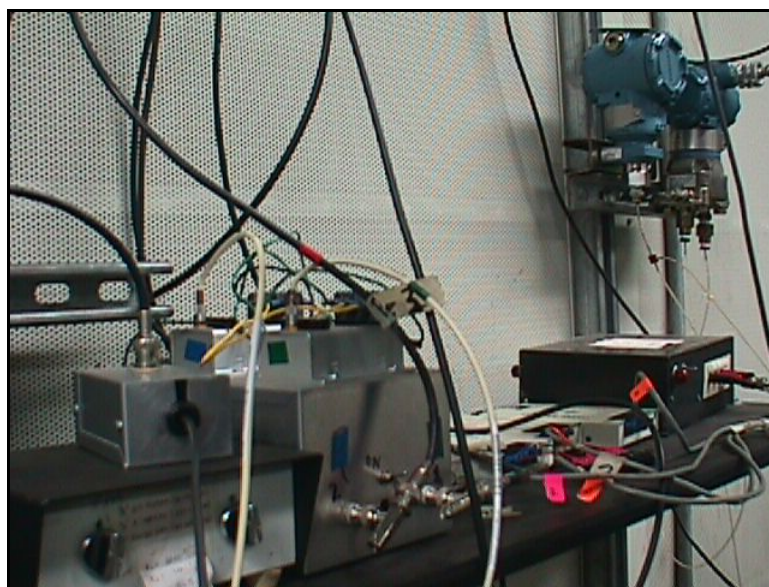
Figure A12: Instrumentation for Data Collection
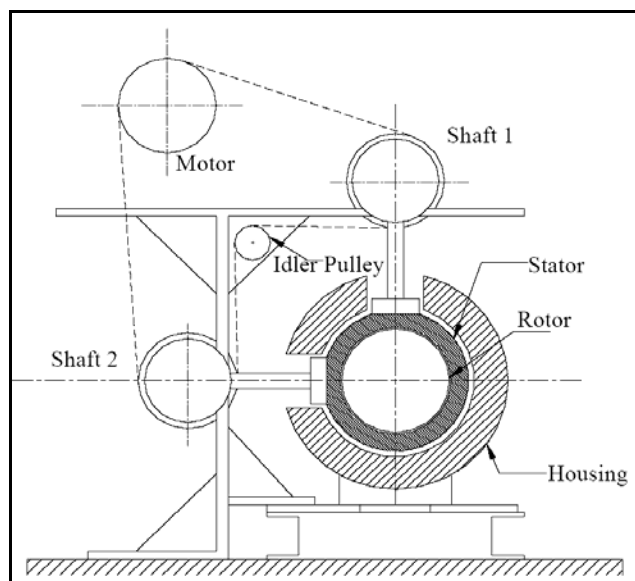
Figure A13: AutoCAD Sketch of Test Rig with Whirl Set-up

Table A1: Axial Downstream Positions of Kulite Transducers on the Brass Block

Kulite Positions (z/L)				
	A	B	C	D
Top	-0.29429	-0.23429	-0.12429	-0.07643
	0.035714	0.095	0.224286	0.286429
	0.407143	0.815714	0.573571	0.635714
	0.767857		0.925714	0.979286
Bottom	0.033571	-0.01714		-0.17857
	0.390714	0.705		0.163571
	0.764286	1.033571		0.512857
	1.087857			0.87

APPENDIX B

PHASE AVERAGED WALL-PRESSURE DISTRIBUTIONS AND WHIRL ORBITS
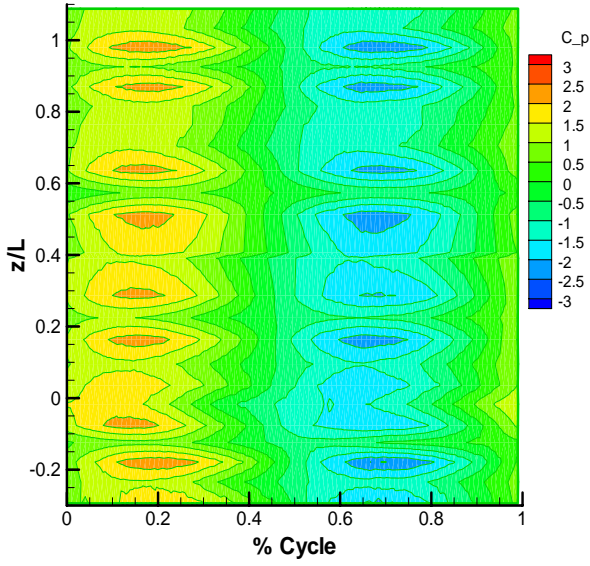
Figure B1: Phase Averaged Pressure (C_p) Re=24000, ε=25%, Ta=3300, β=0.1
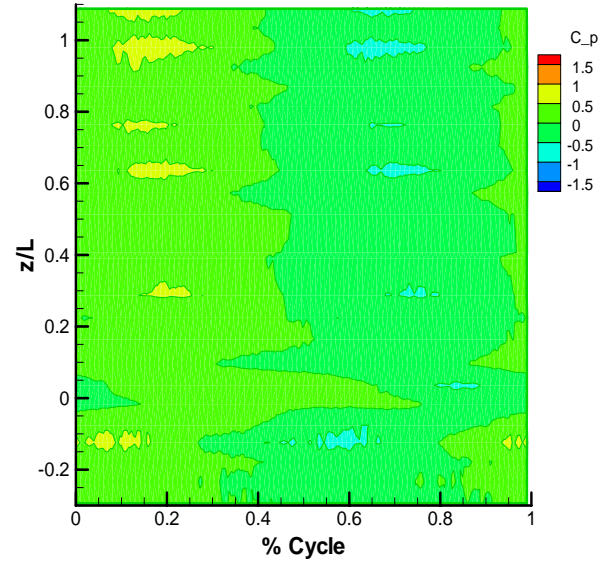
Figure B2: Phase Averaged Pressure (C_p), Re=12000, ε=25%, Ta=3300, β=0.1
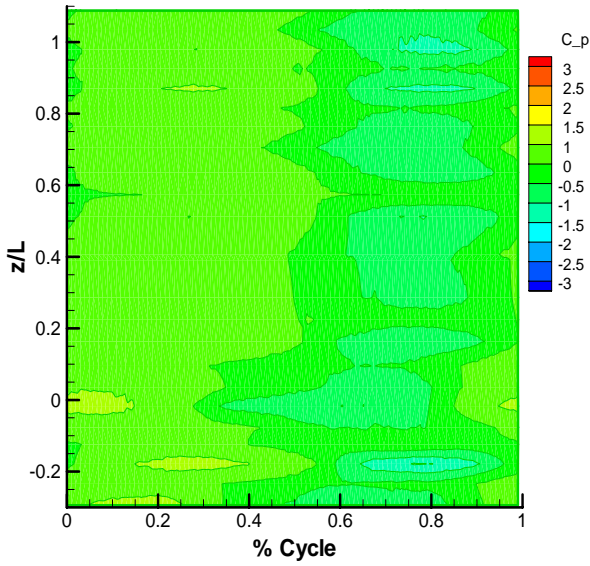
Figure B3: Phase Averaged Pressure (C_p), Re=24000, ε=25%, Ta=3300, β=0.2
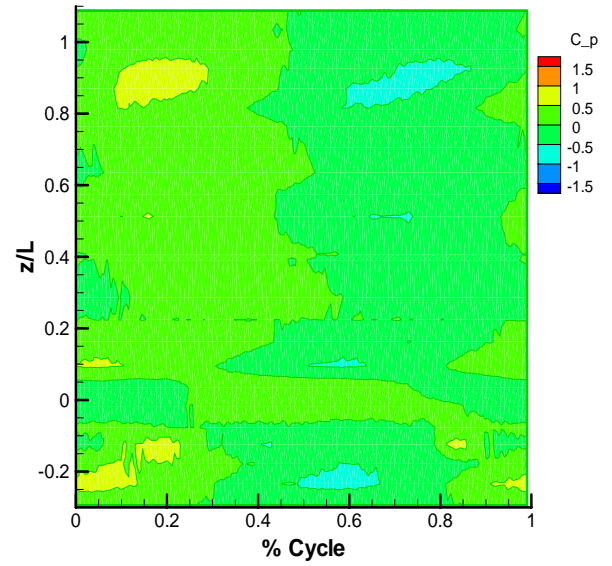
Figure B4: Phase Averaged Pressure (C_p), Re=12000, ε=25%, Ta=3300, β=0.2
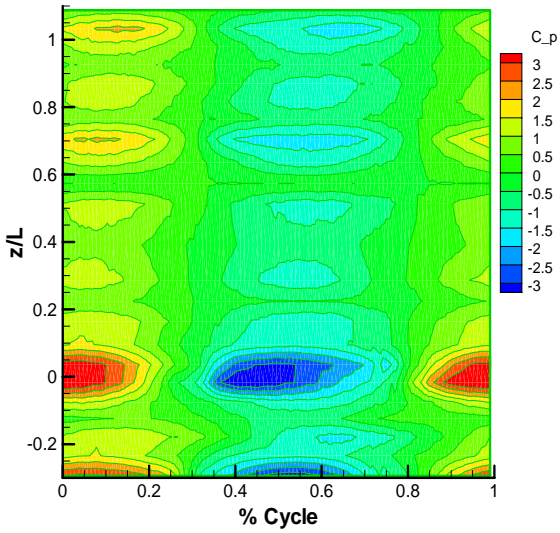
Figure B5: Phase Averaged Pressure (C_p), Re=24000, ε=25%, Ta=3300, β=0.3
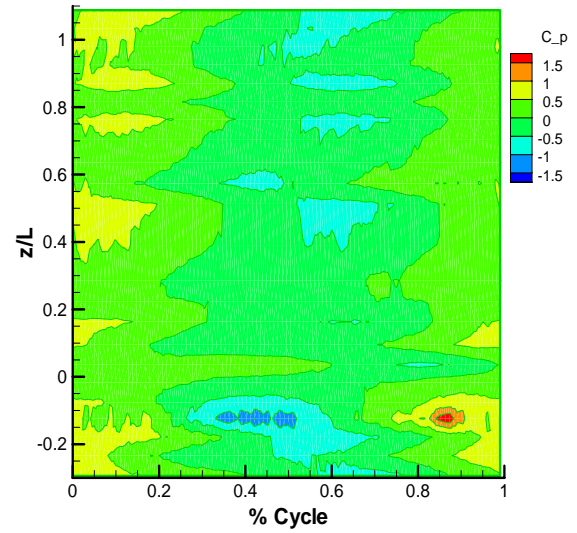
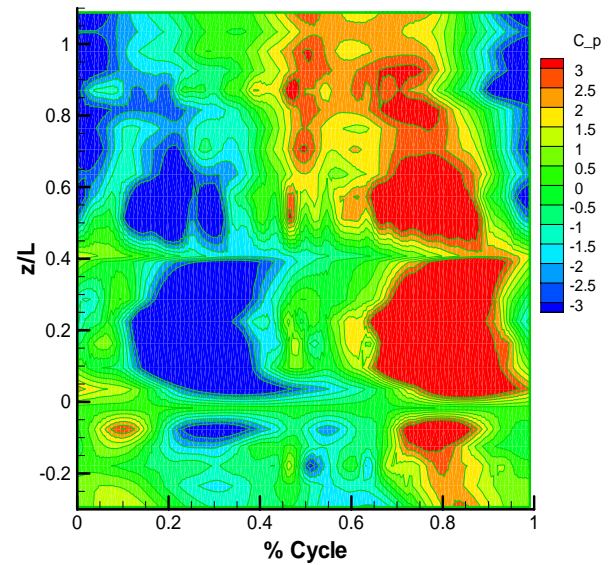**Figure B6: Phase Averaged Pressure (C_p), Re=12000, ε=25%, Ta=3300, β=0.3**
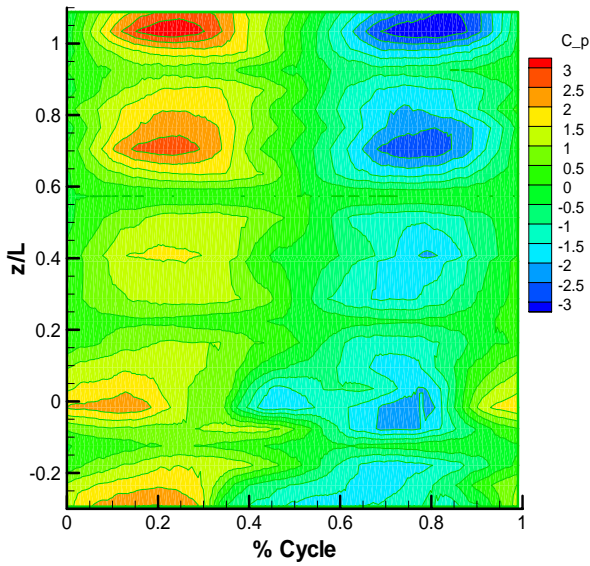
Figure B7: Phase Averaged Pressure (C_p), Re=24000, ε=25%, Ta=3300, β=0.4
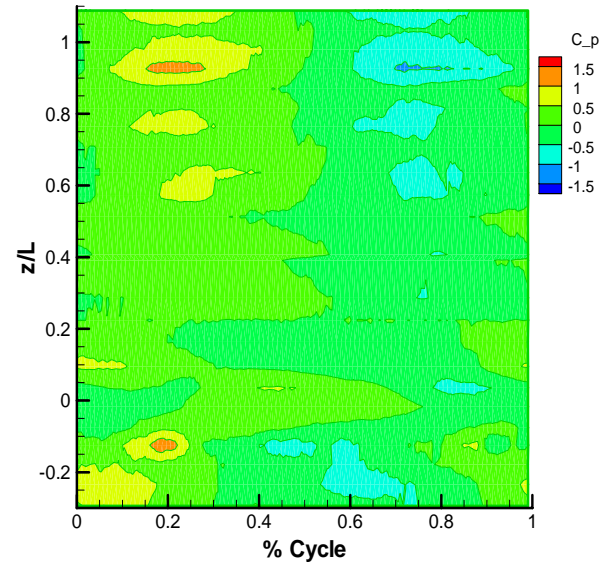
Figure B8: Phase Averaged Pressure (C_p), Re=12000, ε=25%, Ta=3300, β=0.4
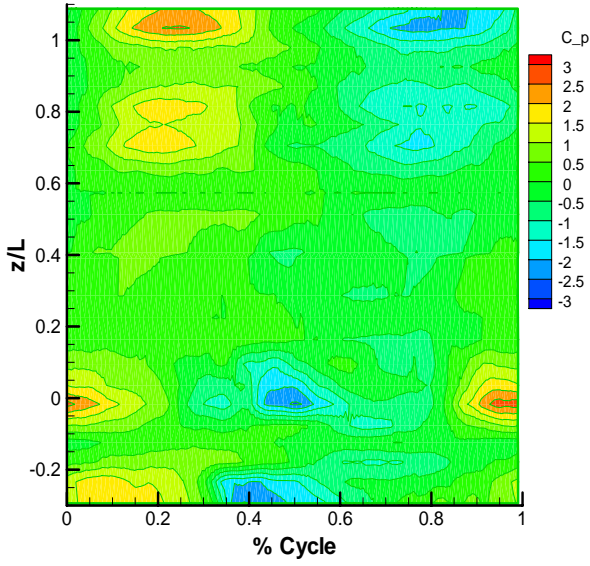
Figure B9: Phase Averaged Pressure (C_p), Re=24000, ε=25%, Ta=3300, β=0.5
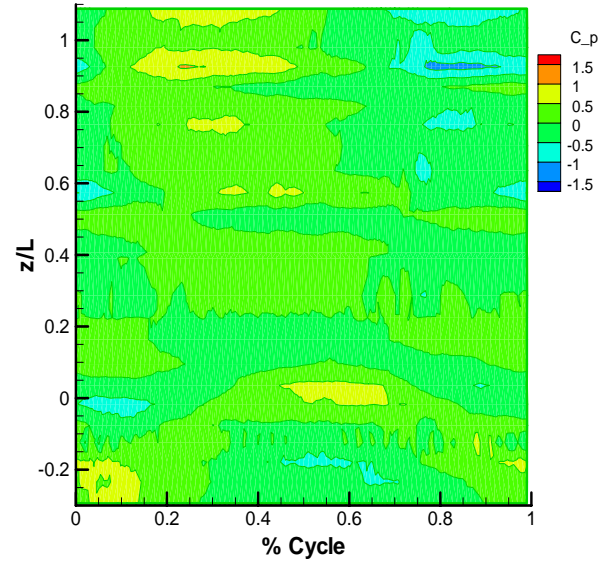
Figure B10: Phase Averaged Pressure (C_P), Re=12000, ε=25%, Ta=3300, β=0.5
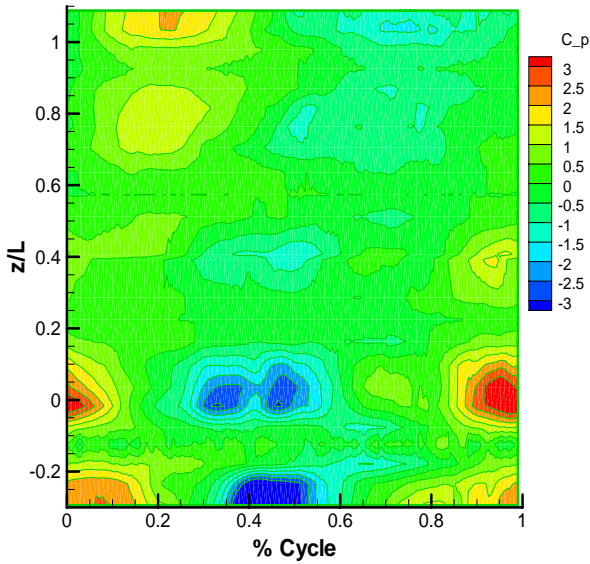
Figure B11: Phase Averaged Pressure (C_p), Re=24000, ε=25%, Ta=3300, β=0.6
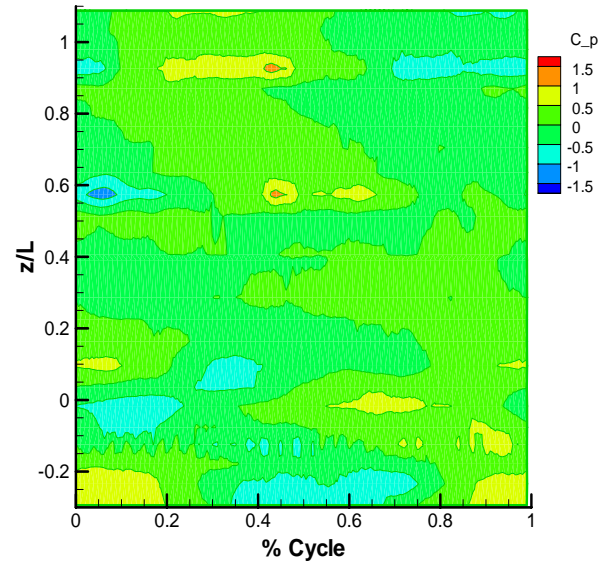
Figure B12: Phase Averaged Pressure (C_p), Re=12000, ε=25%, Ta=3300, β=0.6
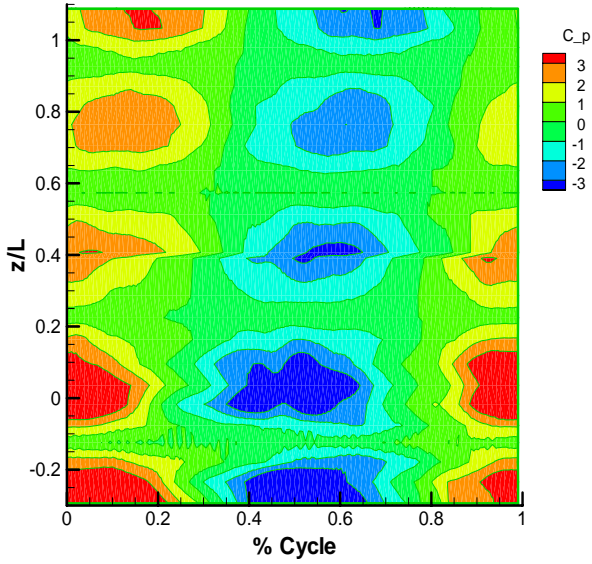
Figure B13: Phase Averaged Pressure (C$_p$), Re=24000, ε=25%, Ta=3300, β=0.7
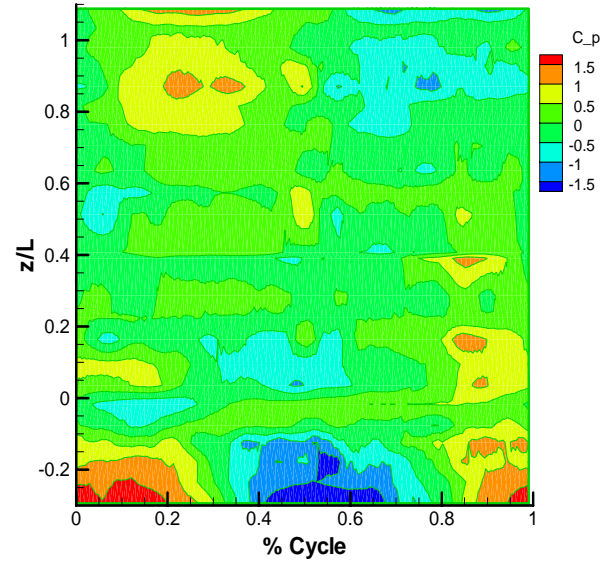
Figure B14: Phase Averaged Pressure (C$_p$), Re=12000, ε=25%, Ta=3300, β=0.7
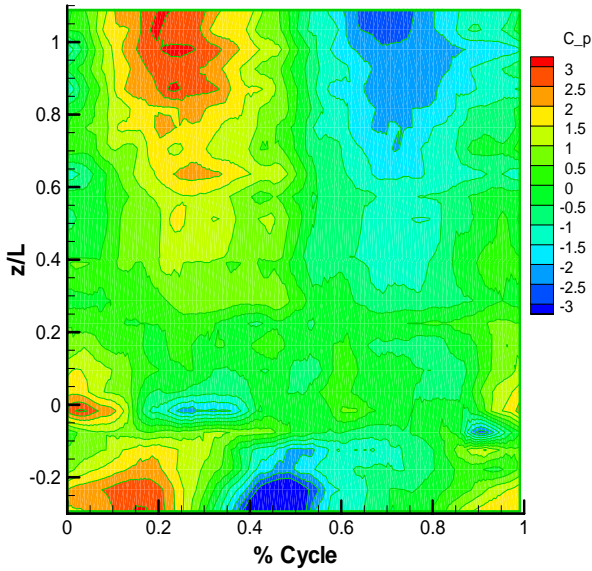
Figure B15: Phase Averaged Pressure (C$_p$), Re=24000, ε=25%, Ta=3300, β=0.8
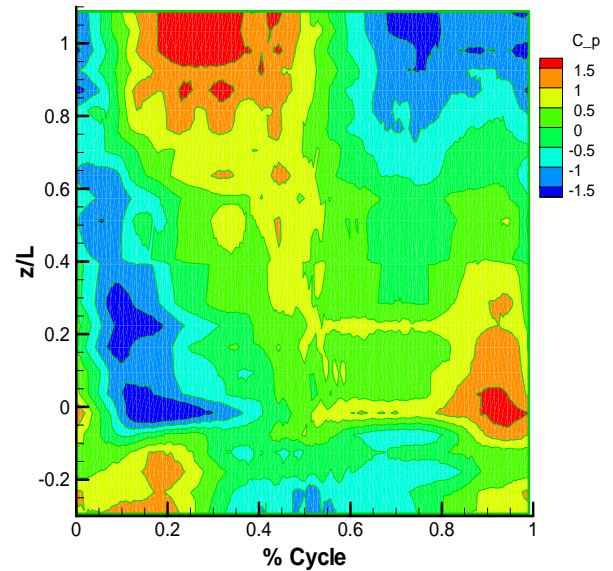
Figure B16: Phase Averaged Pressure (C$_p$), Re=12000, ε=25%, Ta=3300, β=0.8
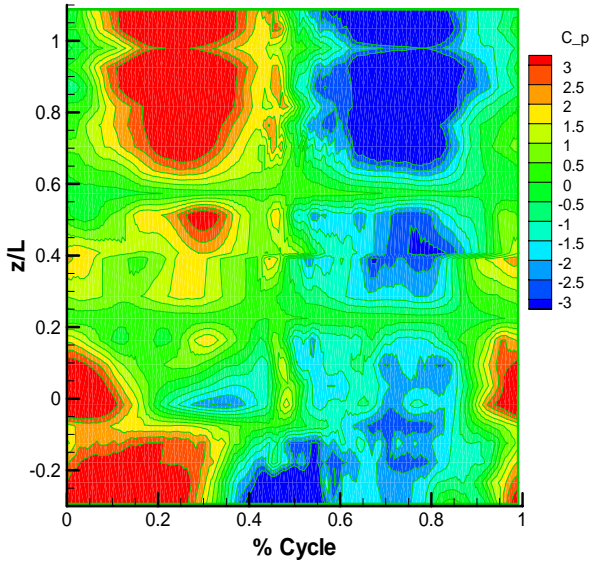
**Figure B17: Phase Averaged Pressure
(C$_p$), Re=24000, ε=25%, Ta=3300, β=0.9**
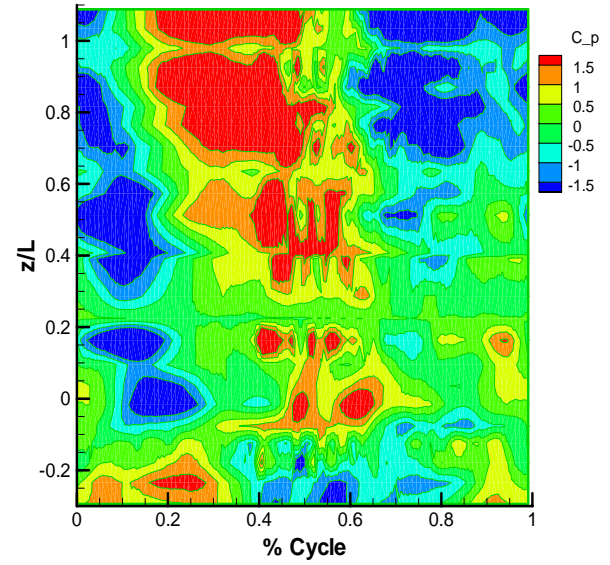
**Figure B18: Phase Averaged Pressure
(C$_p$), Re=12000, ε=25%, Ta=3300, β=0.9**
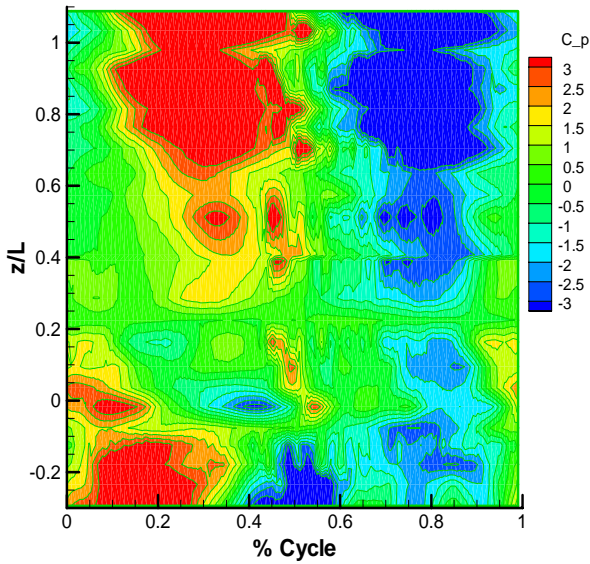
**Figure B19: Phase Averaged Pressure
(C$_p$), Re=24000, ε=25%, Ta=3300, β=1.0**
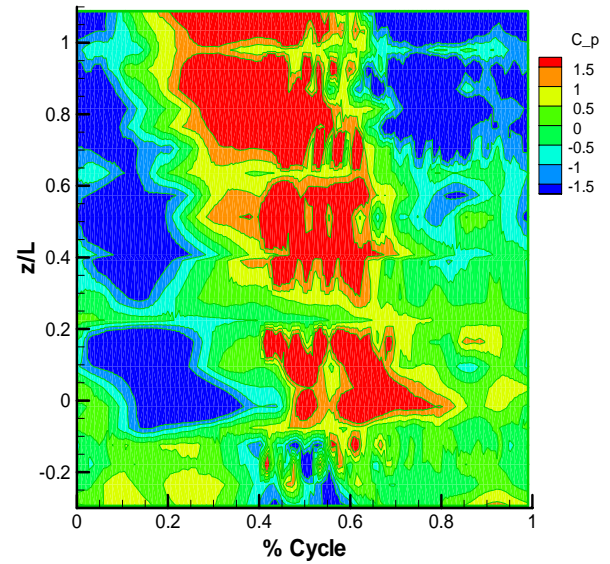
**Figure B20: Phase Averaged Pressure
(C$_p$), Re=12000, ε=25%, Ta=3300, β=1.0**
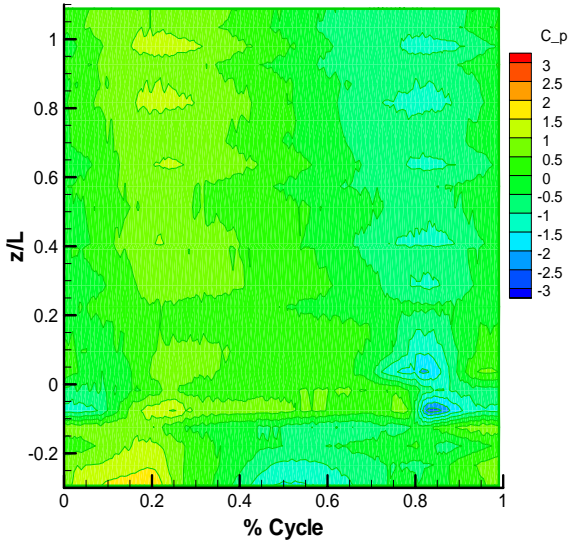
Figure B21: Phase Averaged Pressure (C$_p$), Re=24000, ε=25%, Ta=6600, β=0.1
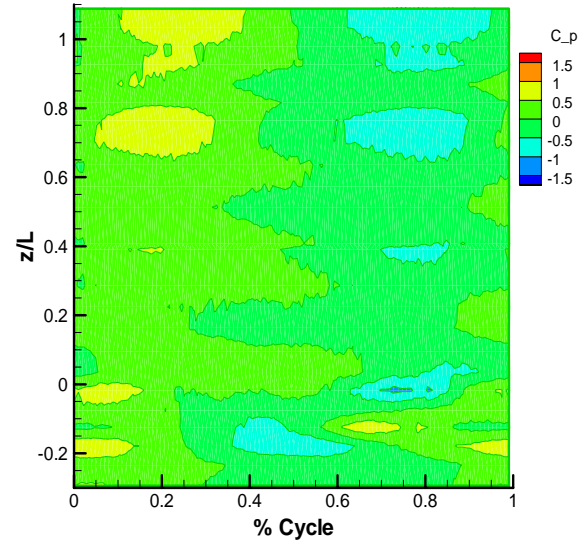
Figure B22: Phase Averaged Pressure (C$_p$), Re=12000, ε=25%, Ta=6600, β=0.1
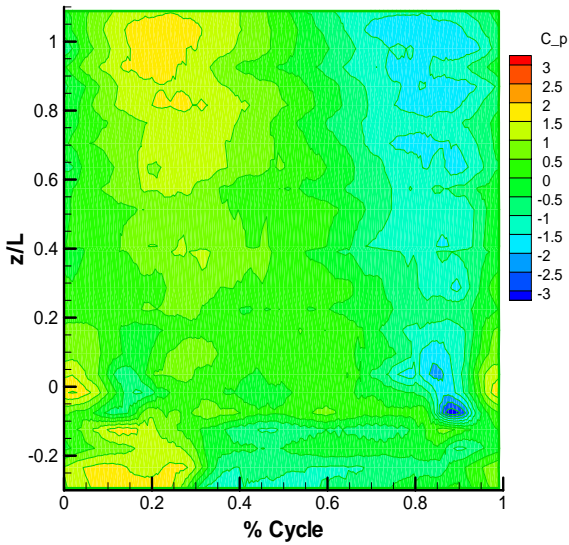
Figure B23: Phase Averaged Pressure (C$_p$), Re=24000, ε=25%, Ta=6600, β=0.2
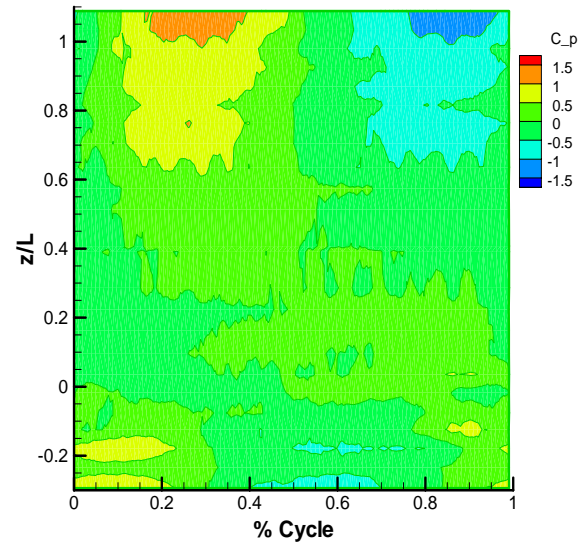
Figure B24: Phase Averaged Pressure (C$_p$), Re=12000, ε=25%, Ta=6600, β=0.2
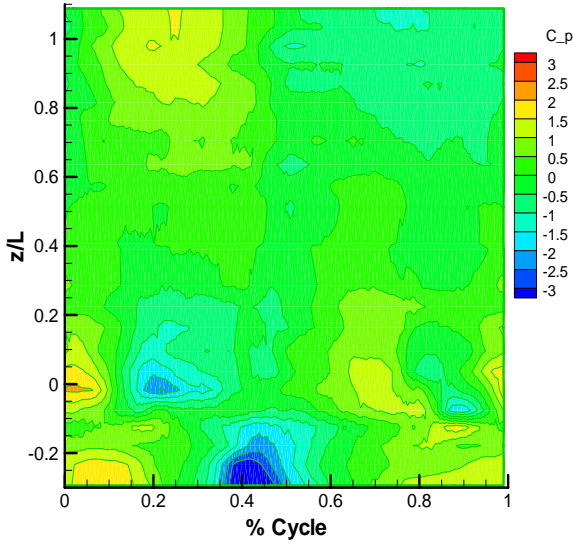
Figure B25: Phase Averaged Pressure (C_p), Re=24000, ε=25%, Ta=6600, β=0.3
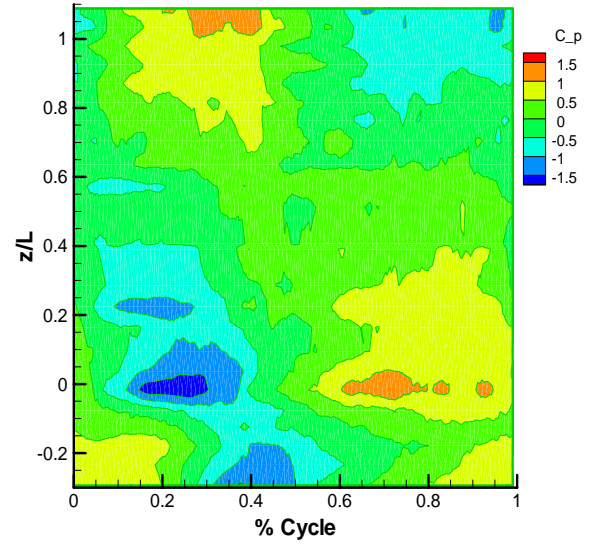
Figure B26: Phase Averaged Pressure (C_p), Re=12000, ε=25%, Ta=6600, β=0.3
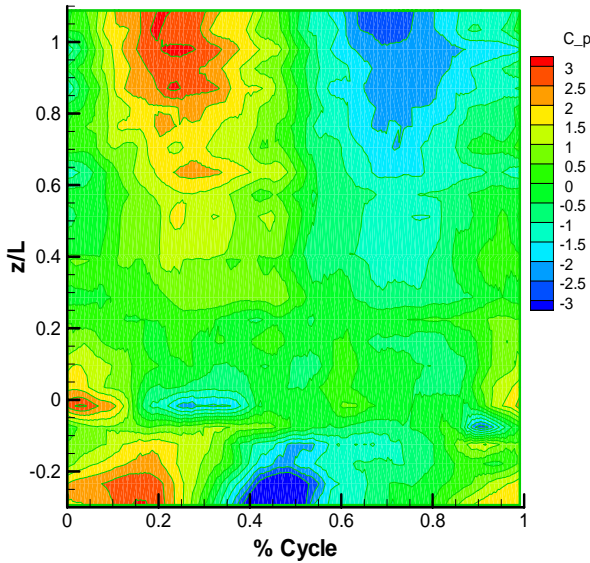
Figure B27: Phase Averaged Pressure (C_p), Re=24000, ε=25%, Ta=6600, β=0.4
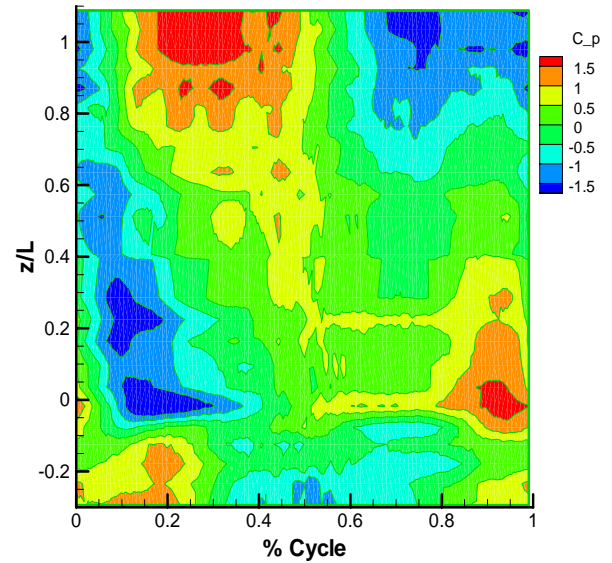
Figure B28: Phase Averaged Pressure (C_p), Re=12000, ε=25%, Ta=6600, β=0.4
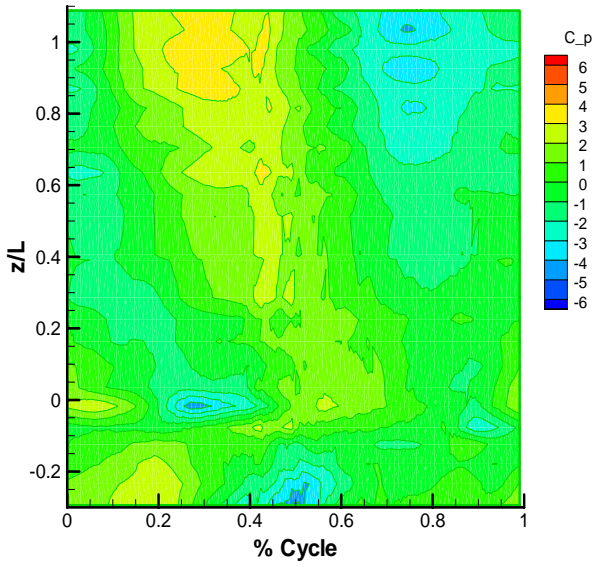
Figure B29: Phase Averaged Pressure (C$_p$), Re=24000, ε=25%, Ta=6600, β=0.5
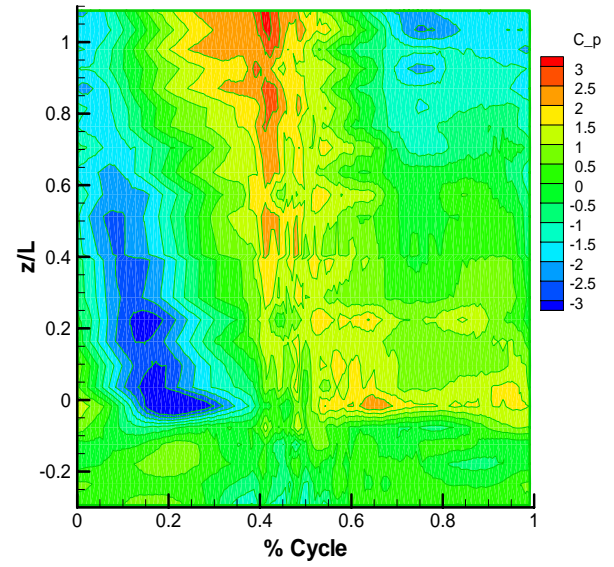
Figure B30: Phase Averaged Pressure (C$_p$), Re=12000, ε=25%, Ta=6600, β=0.5
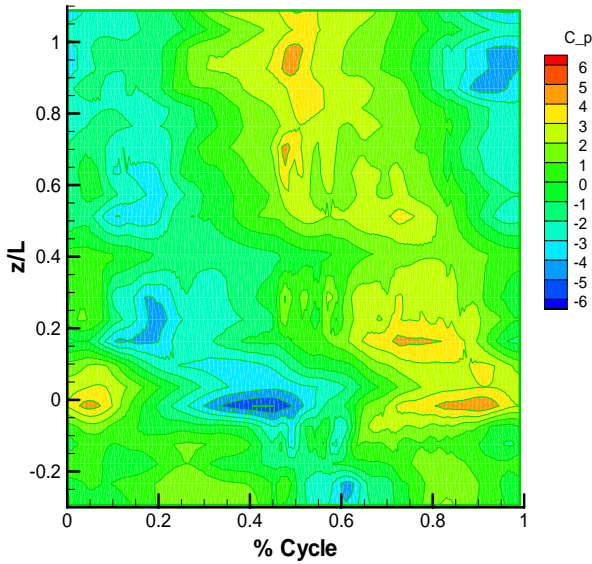
Figure B31: Phase Averaged Pressure (C$_p$), Re=24000, ε=25%, Ta=6600, β=0.6
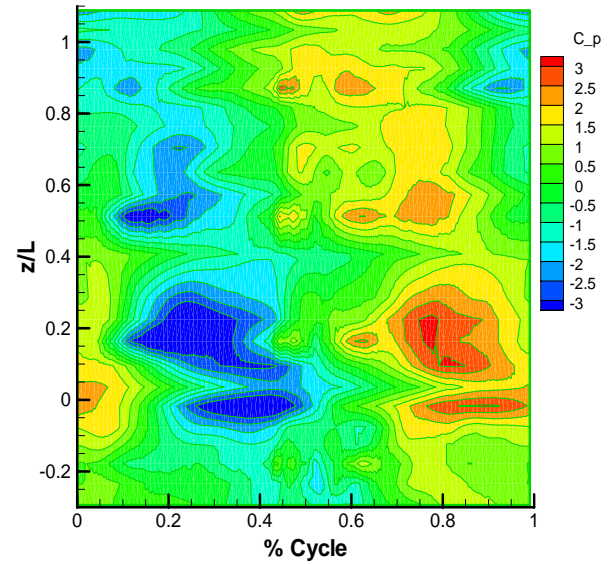
Figure B32: Phase Averaged Pressure (C$_p$), Re=12000, ε=25%, Ta=6600, β=0.6
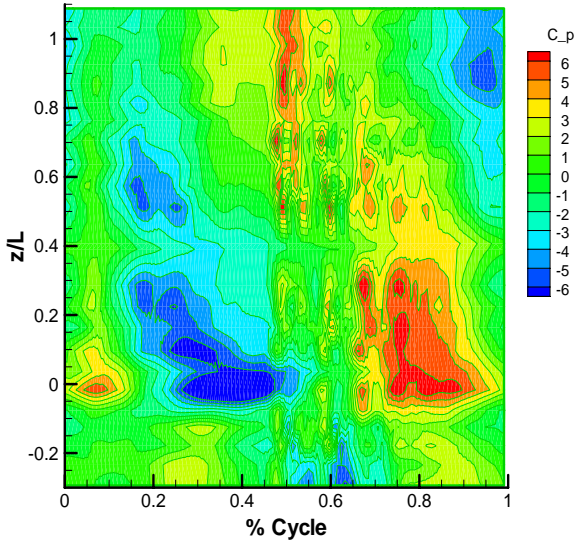
Figure B33: Phase Averaged Pressure (C$_p$), Re=24000, e=25%, Ta=6600, β=0.7
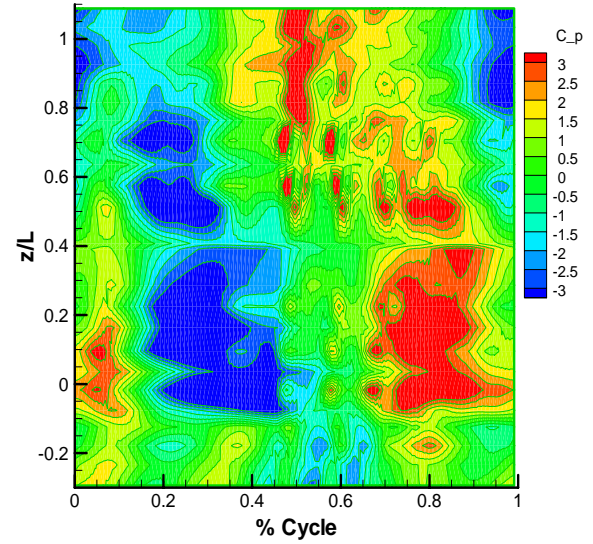
Figure B34: Phase Averaged Pressure (C$_p$), Re=12000, ε=25%, Ta=6600, β=0.7
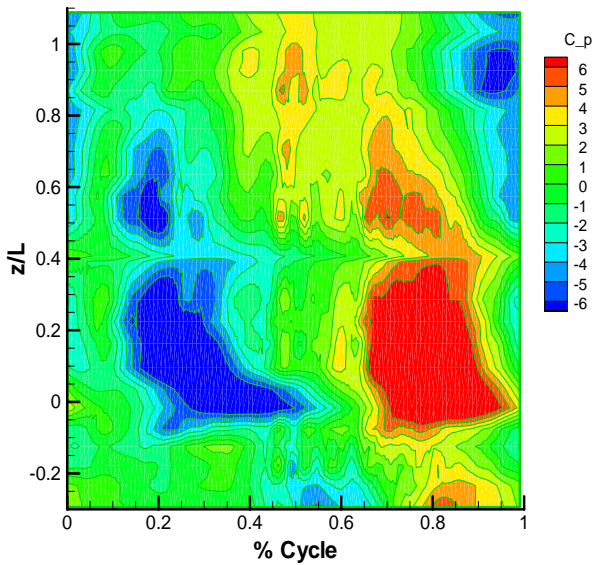
Figure B35: Phase Averaged Pressure (C$_p$), Re=24000, ε=25%, Ta=6600, β=0.8

Figure B36: Phase Averaged Pressure (C$_p$), Re=12000, ε=25%, Ta=6600, β=0.8
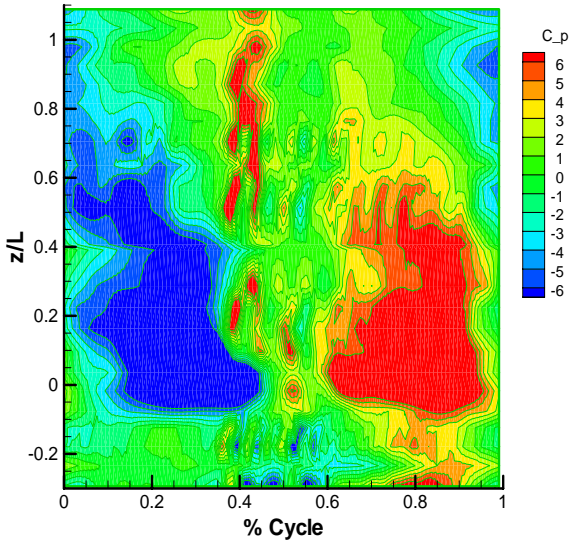
Figure B37: Phase Averaged Pressure (Cₚ), Re=24000, ε=25%, Ta=6600, β=0.9
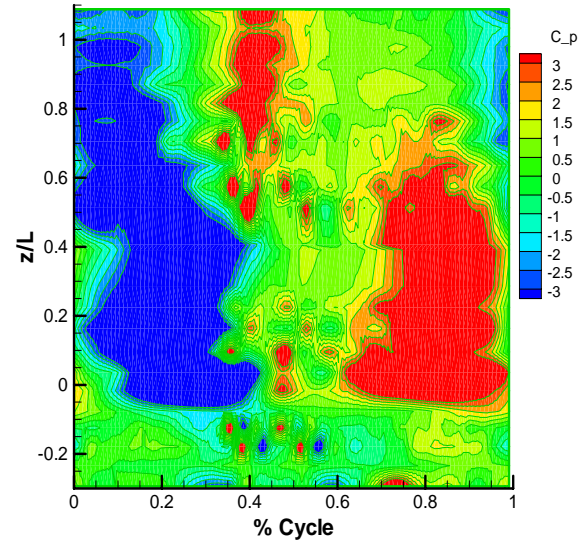
Figure B38: Phase Averaged Pressure (Cₚ), Re=12000, ε=25%, Ta=6600, β=0.9
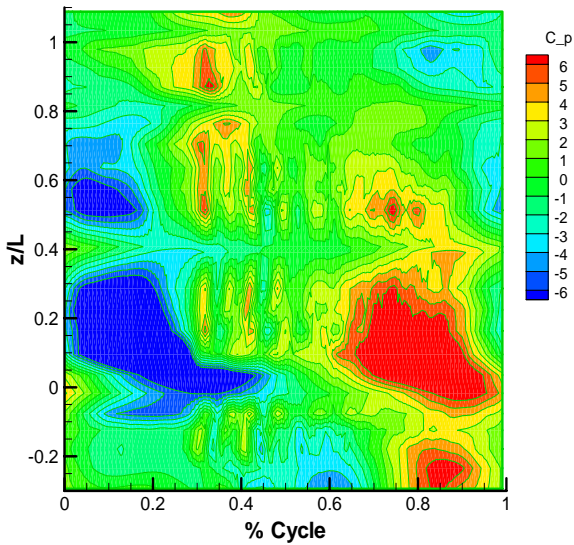
Figure B39: Phase Averaged Pressure (Cₚ), Re=24000, ε=25%, Ta=6600, β=1.0
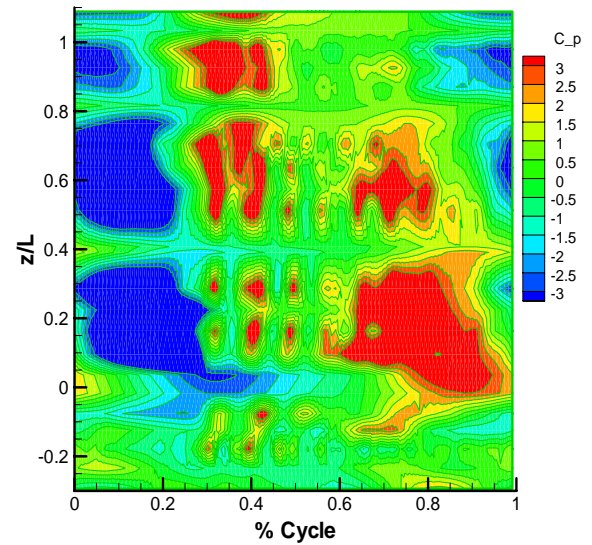
Figure B40: Phase Averaged Pressure (Cₚ), Re=12000, ε=25%, Ta=6600, β=1.0
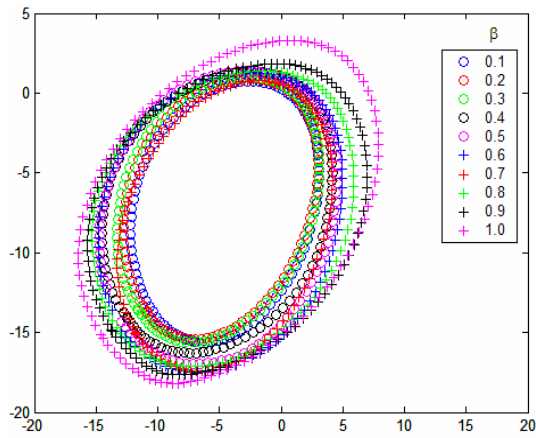
**Figure B41: Seal Orbit in mils
(Ta=3300, Re=24000)**
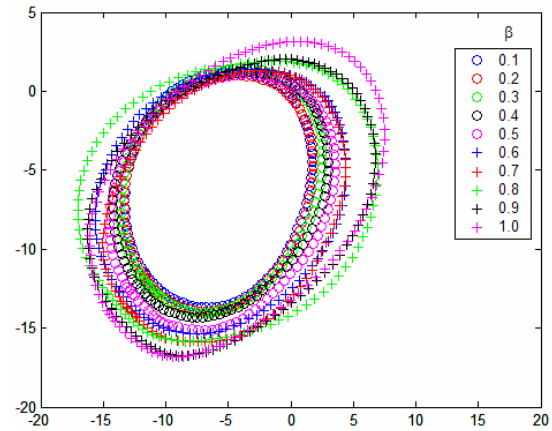
**Figure B42: Seal Orbit in mils
(Ta=3300, Re=12000)**
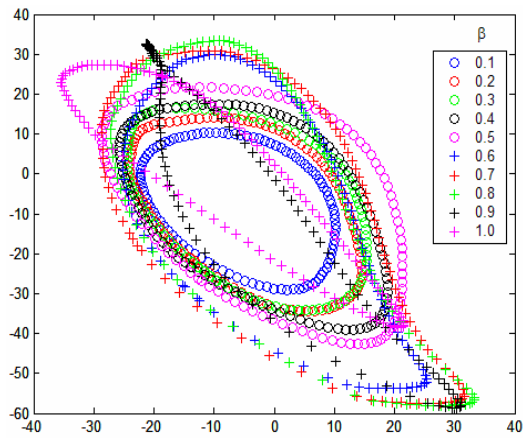
**Figure B43: Seal Orbit in mils
(Ta=6600, Re=24000)**
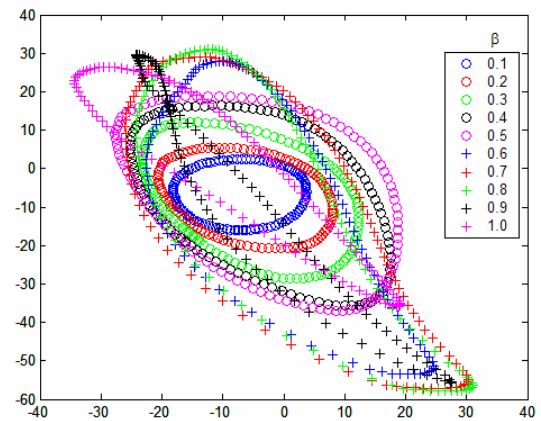
**Figure B44: Seal Orbit in mils
(Ta=6600, Re=12000)**

Table B1: Pressure Drop across Seal [psi]

Whirl Ratio	Operating Conditions			
	1800RPM Re=24000	1800RPM Re=12000	3600RPM Re=24000	3600RPM Re=12000
0.1	4.4798	1.5965	6.9741	2.2486
0.2	4.6551	1.6399	7.0035	2.3702
0.3	4.3211	1.6363	6.9073	2.5845
0.4	4.3499	1.5924	7.1049	2.9380
0.5	4.2599	1.5366	7.6940	3.4459
0.6	4.2022	1.4839	7.9956	3.6662
0.7	4.1693	1.4677	9.0794	5.2440
0.8	4.4699	1.6092	10.5021	3.3077
0.9	4.5367	1.8714	11.1691	4.5827
1.0	4.7470	2.0829	9.7448	3.7275

APPENDIX C

ROTORDYNAMIC FORCE COEFFICIENT PLOTS
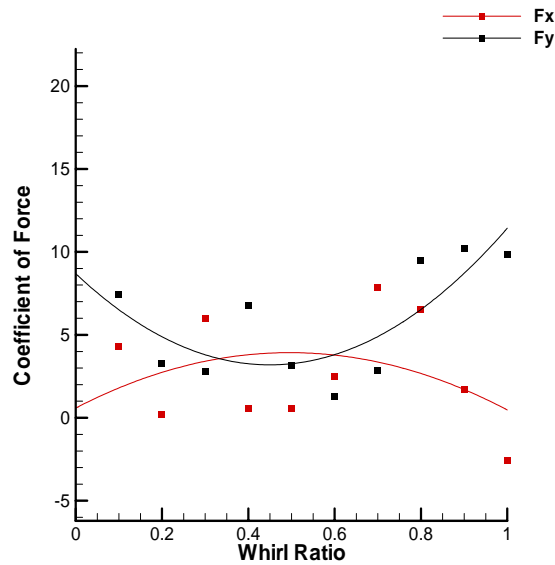
Figure C1: Rotordynamic Coefficient of Force; 0.1 ≤ β ≤ 1.0 (Ta=3300, Re=24000)
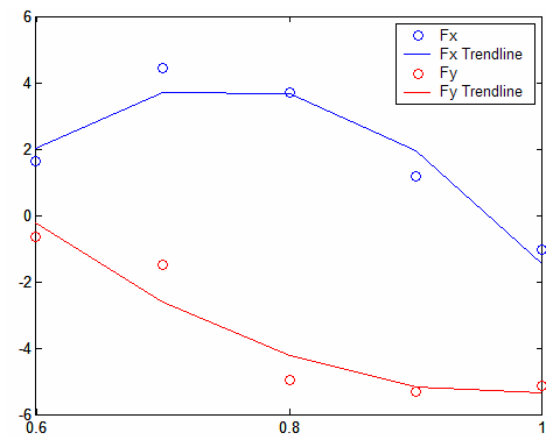
Figure C2: Rotordynamic Coefficient of Force; β ≥ 0.6 (Ta=3300, Re=24000)
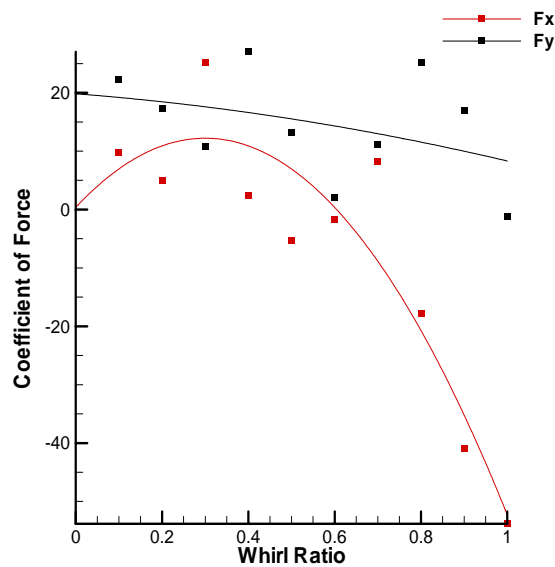
Figure C3: Rotordynamic Coefficient of Force; 0.1 ≤ β ≤ 1.0 (Ta=3300, Re=12000)
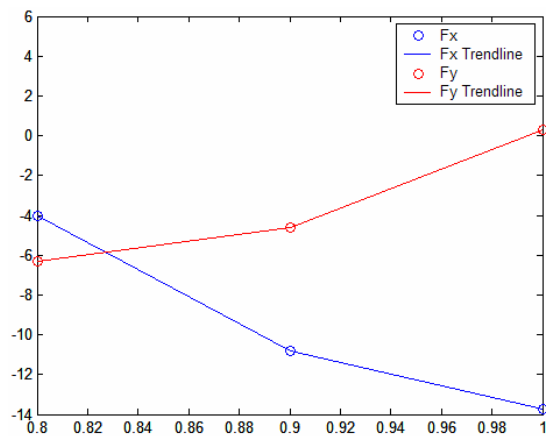
Figure C4: Rotordynamic Coefficient of Force; β ≥ 0.8 (Ta=3300, Re=12000)
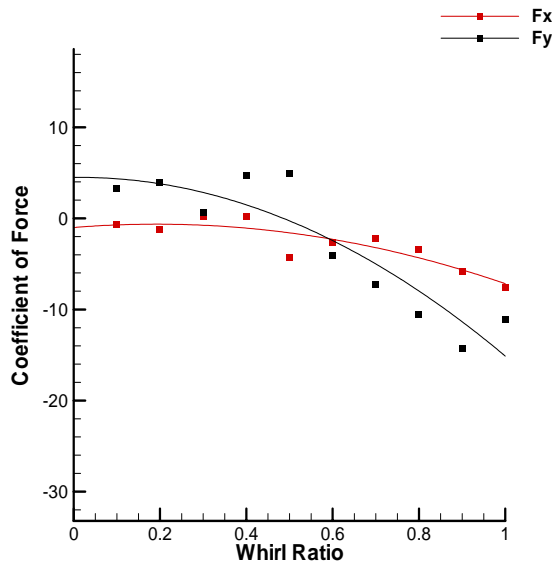
Figure C5: Rotordynamic Coefficient of Force; $0.1 \leq \beta \leq 1.0$ (Ta=6600, Re=24000)
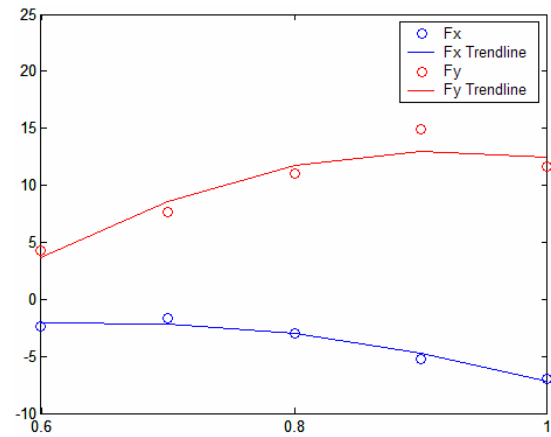
Figure C6: Rotordynamic Coefficient of Force; $\beta \geq 0.6$ (Ta=6600, Re=24000)
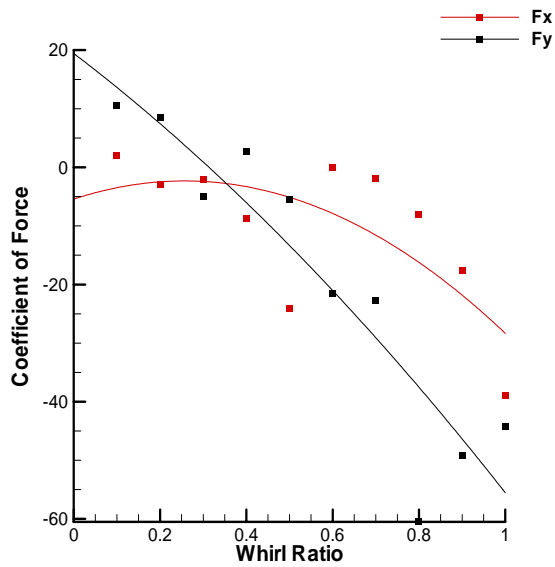
Figure C7: Rotordynamic Coefficient of Force; $0.1 \leq \beta \leq 1.0$ (Ta=6600, Re=12000)
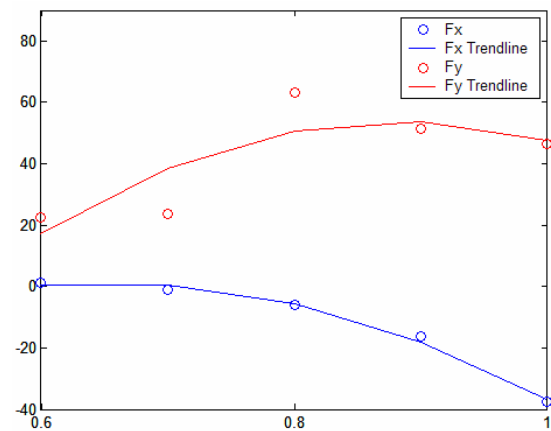
Figure C8: Rotordynamic Coefficient of Force; $\beta \geq 0.6$ (Ta=6600, Re=12000)

APPENDIX D

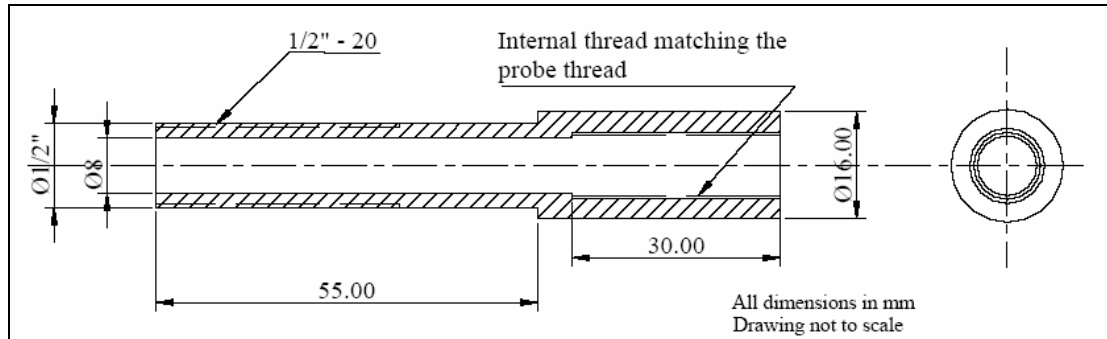**AUTOCAD DRAWINGS OF WHIRL AND ECCENTRICITY SETTING UNIT**
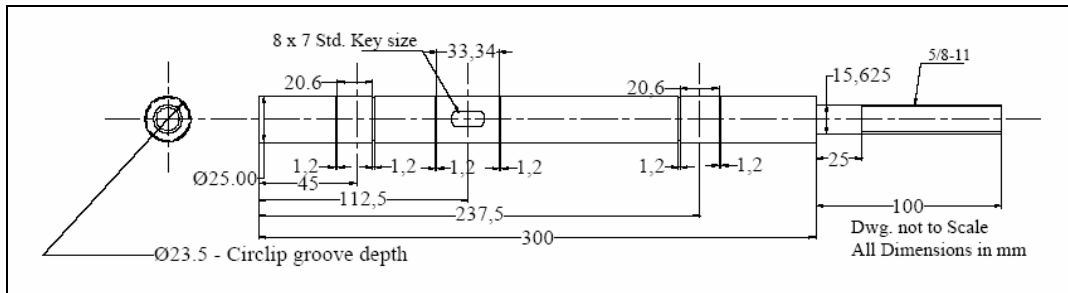
Figure D1: Whirl Shaft

Figure D2: Proximity Probe Adaptor
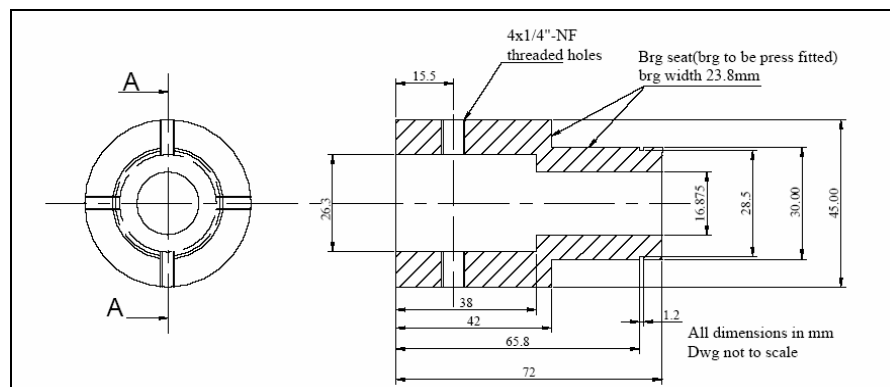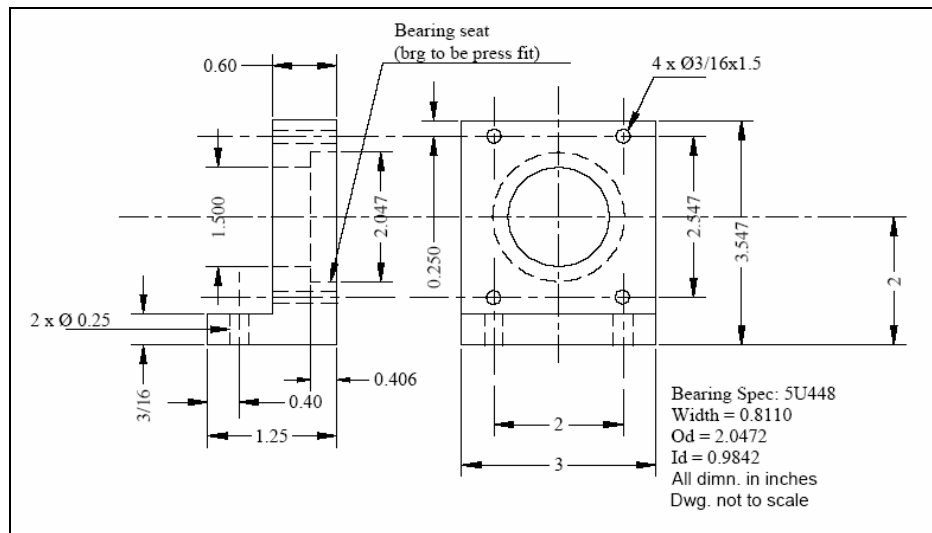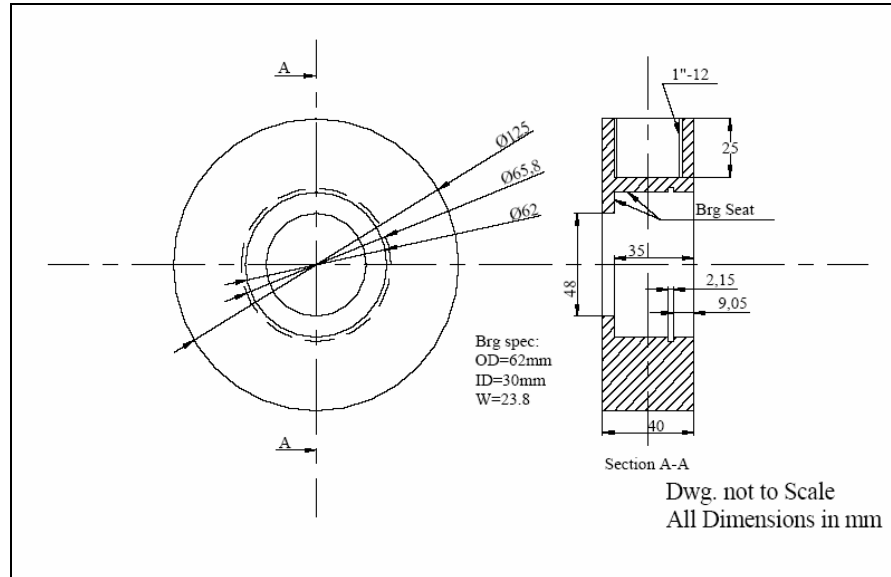

Figure D3: Whirl Cam

Figure D4: Pillow Block

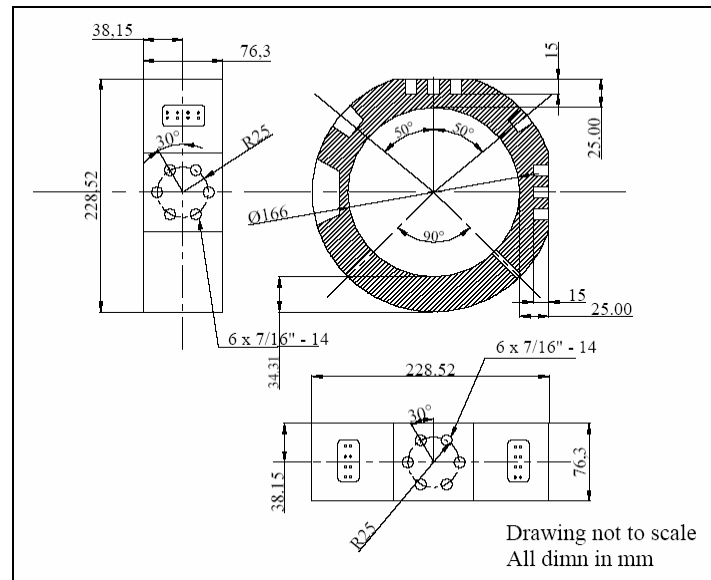**Figure D5: Cam Housing**

Figure D6: Modified Stator

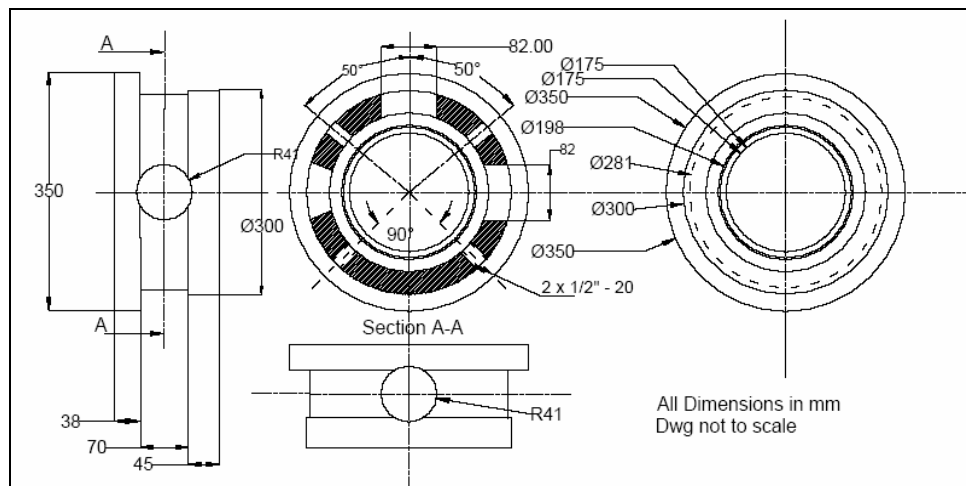**Figure D7: Modified Housing**
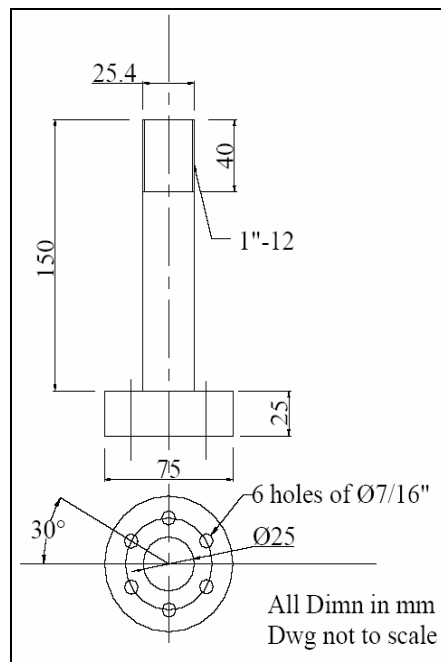
Figure D8: Plunger

VITA

Name: Domenic Cusano

Address: IRC North America LP, 10497 Town & Country Way Suite 800,

                    Houston, TX 77024

Email Address: cusano13@yahoo.com

Education: B.S., Mechanical Engineering, Texas A&M University, College

                    Station, May 2004